geosciences

MDPI

Article

Latest Pleistocene and Holocene Floodplain Evolution in Central Europe—Insights from the Upper Unstrut Catchment (NW-Thuringia/Germany)

André Kirchner [1,*,†], Jasmin Karaschewski [1,†], Philipp Schulte [2], Tina Wunderlich [3] and Tobias Lauer [4,5]

1 Department of Geography, University of Hildesheim, 31141 Hildesheim, Germany
2 Department of Geography, RWTH Aachen University, 52056 Aachen, Germany
3 Institute of Geoscience, Christian-Albrechts-University of Kiel, 24118 Kiel, Germany
4 Department of Geosciences, University of Tübingen, 72072 Tübingen, Germany
5 Department of Human Evolution, Max Planck Institute for Evolutionary Anthropology, 04103 Leipzig, Germany
* Correspondence: andre.kirchner@uni-hildesheim.de
† These authors contributed equally to this work.

Abstract: The upper Unstrut River is located in Germany at the modern Central European climate boundary of Cfb and Dfb climate. The river drains a loess landscape, which has experienced important environmental changes throughout the last 12,000 years. To evaluate the impacts of these changes on floodplain evolution, a multi-proxy research program, consisting of 2D electrical resistivity tomography profiling (ERT), vibracoring, and sedimentological investigations, ^{14}C and OSL dating were applied. From base to top the investigations the following fluvial deposits were revealed: (1) gravels embedded in a fine-grained sediment matrix (interpreted as fluvial bedload deposits); (2) silty sediment with pedogenic features (interpreted as overbank floodplain deposits); (3) peat and tufa deposits (interpreted as wetland deposits) intercalated by pedogenetically influenced silty sediments (interpreted as overbank deposits); (4) humic silty sediment with some pedogenic features (interpreted as overbank floodplain deposits); and (5) silty sediments (interpreted as overbank deposits). Radiocarbon and luminescence dates yielded the following periods for sediment formation: (1) Younger Dryas to Preboreal period (around 11.6 cal ka BP); (2) Preboreal to early Atlantic period (approx. 11.6 to 7.0 cal ka BP); (3) early Atlantic to late Subboreal period (approx. 7.3 to 3.4 cal ka BP); (4) late Subboreal to early Subatlantic period (2.9 to 2.3 cal ka BP); and (5) late Subatlantic period (approx. 1.0 to 0.6 cal ka BP). The results suggest that floodplain development during the latest Pleistocene and early Holocene (approx. 11.6 to 7.0 cal ka BP) was considerably controlled by climatic conditions and short-term climate variabilities, which caused gravel deposition and overbank sedimentation. Afterwards floodplain conditions varied between rather stable (peat and tufa development, initial soil formation) and active periods (deposition of overbank fines). In this context, active periods with increased sediment input prevailed from approx. 5.1 to 3.4 cal ka BP, 2.9 to 2.3 cal ka, and 1.0 to 0.6 cal ka BP, temporally corresponding well with increased land-use phases of the past. In conclusion this study demonstrates that the investigated Unstrut catchment has reacted very sensitively to natural and human-induced changes during the latest Pleistocene and Holocene. Consequently, this high vulnerability to external changes should be considered in future river predictions or river management.

Keywords: floodplain evolution; Central European climate boundary; ERT; chronostratigraphy; environmental changes; initial soil formation

Citation: Kirchner, A.; Karaschewski, J.; Schulte, P.; Wunderlich, T.; Lauer, T. Latest Pleistocene and Holocene Floodplain Evolution in Central Europe—Insights from the Upper Unstrut Catchment (NW-Thuringia/Germany). *Geosciences* **2022**, *12*, 310. https://doi.org/10.3390/geosciences12080310

Academic Editors: Luisa Sabato and Jesus Martinez-Frias

Received: 11 May 2022
Accepted: 25 July 2022
Published: 19 August 2022

1. Introduction

Sedimentary archives such as loess-palaeosol sequences, lake sediments or fluvial deposits are frequently used to reconstruct geomorphic processes of the past [1–3]. Fluvial

deposits offer information on landscape change in catchment areas and are especially valuable sediment archives of palaeoenvironmental and geomorphic changes during the late Pleistocene and Holocene [4–8]. In western and Central Europe, fluvial sediments of late Pleistocene and Holocene age are abundant and many of the river systems have typical fluvial patterns [9–12]. However, differences between external drivers and individual internal system configurations preclude a straight-forward generalization of Pleistocene–Holocene fluvial development [13–17]. Most previous studies of late Quaternary fluvial development in western and Central European loess landscapes have focused on the influence of natural environmental and anthropogenic changes on fluvial history [9–17]. Fundamental examples include studies of loess regions in Belgium [18–20] and France [21,22], the Wetterau loess basin of Germany [23–25] and the lower Rhine embayment of Germany [26]. Additionally, several studies exist from more continental loess areas of Central Europe, such as the Pleiße and Weiße Elster catchment of Germany [27–30] and the Vistula basin of Poland [31,32]. However, besides some general patterns, smaller scale local configurations are evident and underline the need for further investigation [11].

This paper presents a case study of fluvial development in the upper Unstrut catchment of central Germany (Figure 1), a loess landscape that is located along the modern climatic transitional zone from an oceanic climate to a more continental climate. This work provides robust chronostratigraphic information on the latest Pleistocene and Holocene floodplain evolution. Based on the regional fluvial chronostratigraphy, this investigation evaluates the impacts of natural environmental and anthropogenic changes on floodplain evolution and therefore contributes to a better understanding of fluvial systems in western and Central European loess landscapes.

2. Study Area

2.1. Environmental Setting

The upper Unstrut catchment is located in central Germany (Federal State of Thuringia) and is around 700 km^2 (Figure 1A). The Unstrut River, which is the main river draining the area, originates in the northern Hainich Mountains (Figure 1B). In the headwater area, the Unstrut River is incised into resistant calcareous rocks of Middle Triassic (Muschelkalk) age, and consequently the valley is narrow. The valley expands southeast of the city of Mühlhausen (Figure 1B), where Upper Triassic (Keuper) strata are predominant. These Upper Triassic strata consist mainly of mudstones with intercalated beds of sulphate-rich carbonate (Lower and Middle Keuper) or sandstone and siltstone (Upper Keuper) [33]. In this river section, the valley is rather flat (approx. 1.2‰) and has an average width of approx. 800 m. Several small streams drain into the upper Unstrut River, especially from the neighbouring Hainich Mountains. The Luhne River (A_{eo} approx. 60 km^2) and Notter River (A_{eo} approx. 122 km^2) are the only larger tributaries that notably contribute to the discharge of the Unstrut River (Figure 1B). The Luhne River drains parts of the northern Hainich Mountains and enters the Unstrut River north of Mühlhausen. The Notter River rises in the northeastern Unstrut catchment, entering the Unstrut River southeast of Mühlhausen, an area with Upper Triassic strata.

Especially in gently inclined areas, the Upper Triassic (Keuper) bedrock is covered by Quaternary (Weichselian) loess and loess derivates. According to the European loess map [34], the study area is part of the northern European loess belt, subdomain IIe (Central European low mountain ranges and basins subdomain, Figure 1A). Thermoluminescence dating of the nearby loess-paleosol sequence Körner indicates multi-phase loess accumulation during the Weichselian glaciation, with the youngest accumulation dated at approx. 15 ka [35]. Highly fertile Chernozems and Chernozem-related soils (Haplic, Cambic, Luvic Chernozems, Luvic Phaeozems) developed in the loess deposits during the Holocene [36,37].

The upper Unstrut catchment is located at the modern climate boundary from the Cfb to Dfb climate [38] and experiences humid conditions with a clear precipitation maximum during the summer months. Average annual precipitation data from two nearby climate

stations range between 518 and 597 mm. Average annual temperature is around 8.3 °C [39].

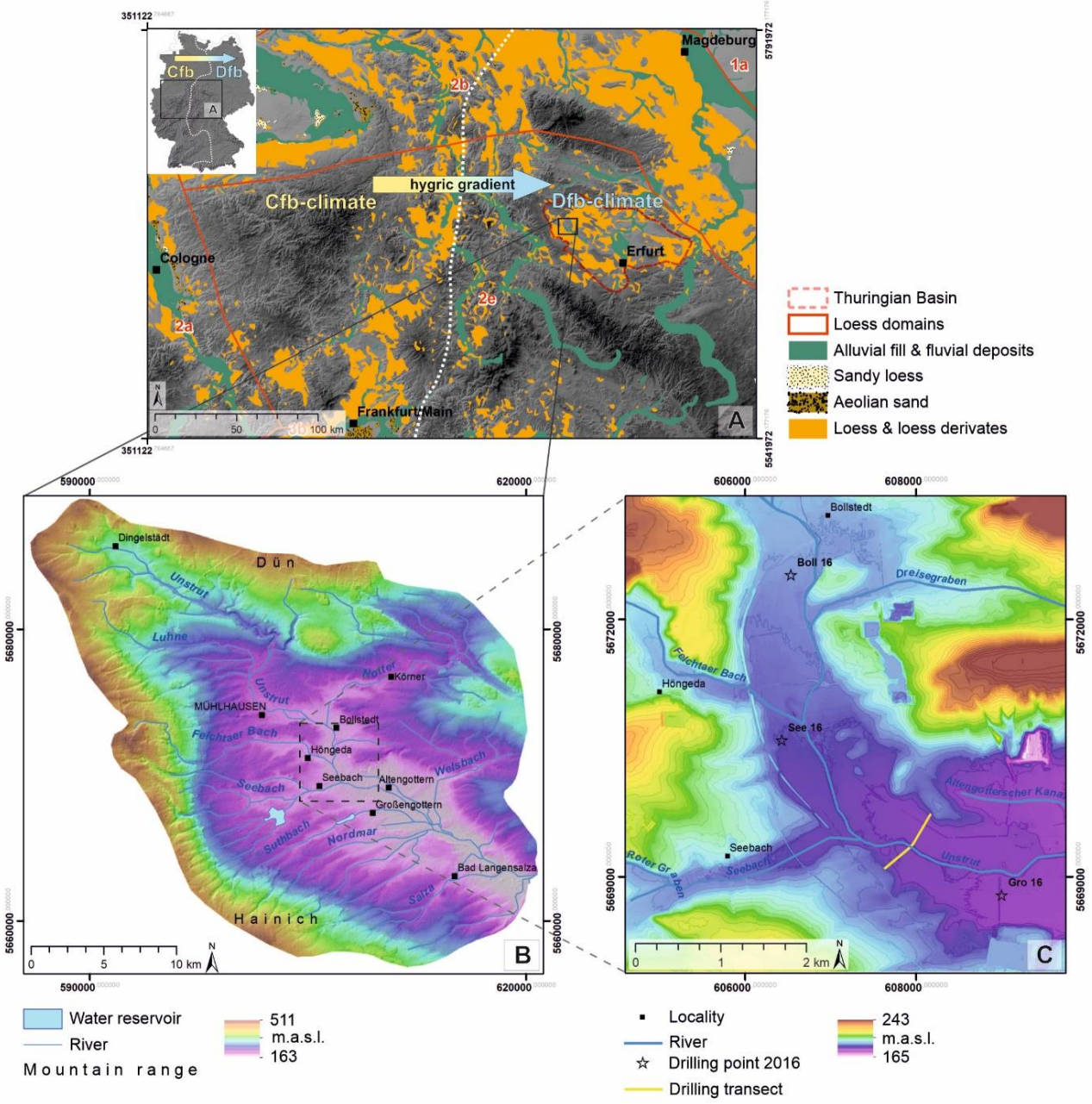

Figure 1. (**A**) Location of the Unstrut catchment of central Germany within a Central European loess landscape, subdomain 2e [34] (DEM200: BKG2018). The meridional climate boundary between Cfb and Dfb climates is indicated by the dotted white line [38]. (**B**) Upper Unstrut catchment from the headwater area near the village of Dingelstädt to the gauging station Nägelstädt (A_{eo} = 716 km^2) (SRTM: USGS, VG250: BKG2018). (**C**) Detailed map of the investigated area southeast of Mühlhausen showing locations of cross-section and initial drillings achieved during 2016 (DEM5: BKG2018). Coordinate system: ETRS 1989 UTM Zone 32N.

2.2. Fundamentals on Unstrut River History

Until 1850 CE, the upper course of the Unstrut River was hardly regulated and the landscape was characterized by meandering river loops and a vegetation of bushes and trees. At this time the floodplain could scarcely be used for agriculture because of the high risk of flooding, and several historically well-documented flooding events are known for the Unstrut catchment [40,41]. After 1861 CE, the river was artificially channelized and diked for flood prevention purposes, enabling agricultural use of the floodplains. Nowadays, the Unstrut River mostly has a straight channel form and flooding events occur rarely.

Knowledge on the sedimentological patterns of the Unstrut valley fillings is mainly derived from investigations undertaken in the 1960s, 1970s, and 1990s [42–48]. According to these studies, the valley floor is frequently formed by gravels that accumulated during the Weichselian Pleniglacial period, locally underlain by older Quaternary sediments. Gravelly deposits are overlain by grey to green silt, which is thought to have accumulated during the late Pleistocene [43]. The silty deposits are covered by heterogonous organic calcareous sediments of the Holocene (Preboreal to Subboreal) age. In Thuringia this heterogonous sequence is known as the "rieth series" [44] and includes complex interbeddings of peat layers and tufa with calcareous and organic clays and silts [48]. The "rieth series" deposits are covered by silty sediments which are interpreted as overbank floodplain fines that accumulated from the Middle Ages to modern times [42,44,47].

2.3. Archaeo-Historical Setting

Similar to many Central European loess areas, the region has almost continuously been settled and used for agriculture since the Neolithic period [49]. Older remains of Palaeolithic and Mesolithic hunter-gatherer communities are rare in the study area, which seems to be the consequence of the low population density and long soil erosion history [50] (Figure 2A). Known early to middle Neolithic sites are mainly concentrated in the smaller tributary valleys of the Unstrut River (Figure 2A). Few data are available for the young Neolithic period, which might be an indication of comparatively low levels of settlement activity. From the late to end Neolithic period, the archaeological sites are increasingly concentrated on the slopes directly bordering the Unstrut (Figure 2A–D). Based on the frequency of archaeological sites, intensive settlement and land-use phases must be assumed for the early, late, and end Neolithic period, the early and late Bronze Age, and the entire Iron Age and Roman Imperial period [50] (Figure 2). During the following Migration Period, the number of archaeological sources decreases considerably, indicating a sharp decline in population. From the early Middle Ages (Merovingian period), the repopulation of the area began (Figure 2D), reaching a climax in the 11th century CE [51]. The settlement foundation went hand in hand with large-scale deforestation and land-use intensification in the corresponding period [52]. However, some of the settlements were abandoned later, especially during the 13th to early 14th centuries CE, which is generally explained by the high concentration of settlements. Declining population and land use can be assumed until about 1450 CE, followed by an increase towards the modern period [51,53]. Striking land-use changes occurred in the 2nd half of the 20th century, when consolidation measures were carried out throughout the territory of the German Democratic Republic (GDR). Agricultural land was gathered together in agricultural production cooperatives. This led to a drastic loss of landscape structures and comparatively large areas of arable land being preserved until today [54].

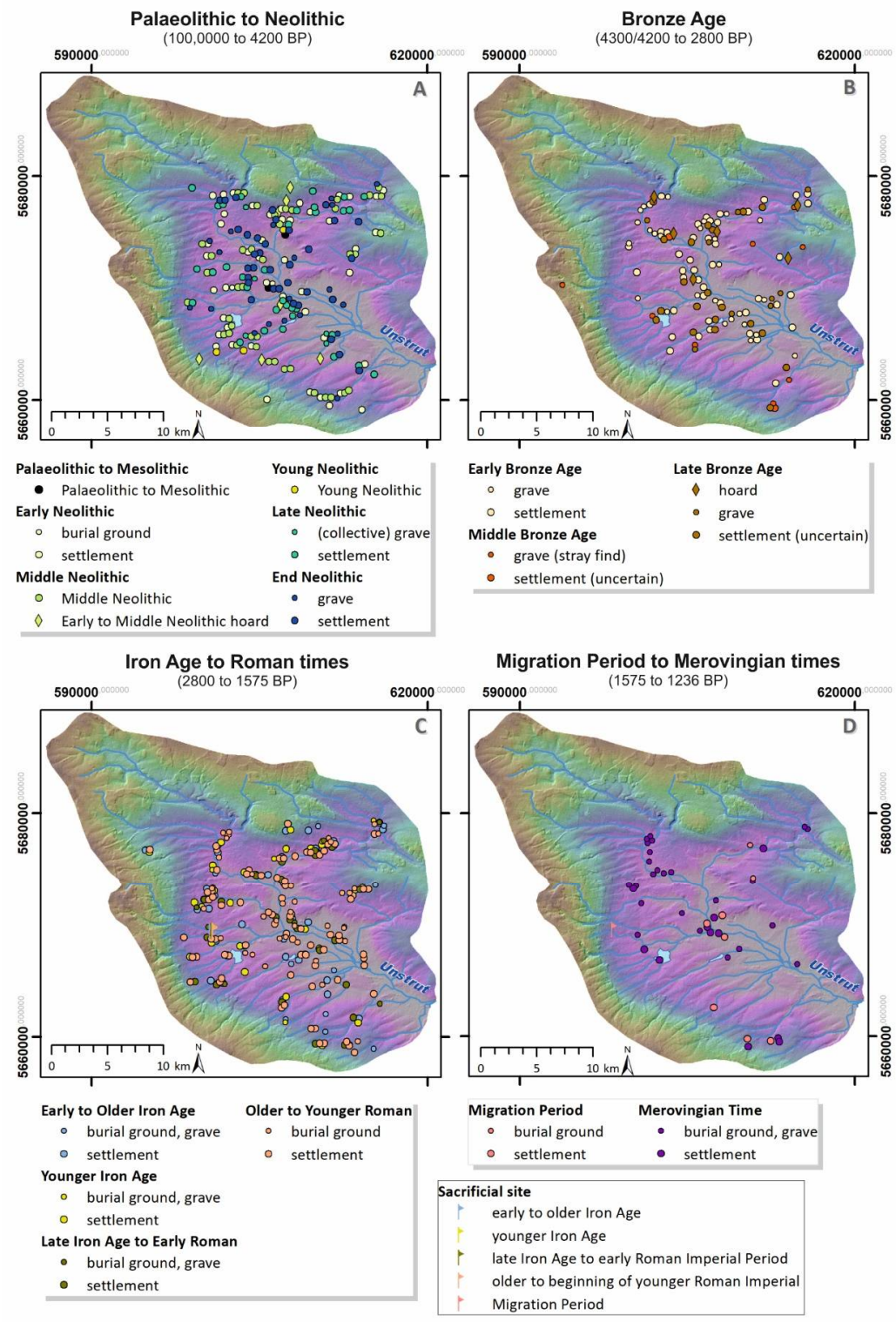

Figure 2. The maps show the upper Unstrut catchment area with 580 known archaeological sites [50] differentiating between (**A**) Palaeolithic to end Neolithic period, (**B**) the Bronze Age, (**C**) early Iron Age to the end of the Roman period, (**D**) the Migration Period to the end of the Merovingian time. Sacrificial sites from the Iron Age onward at the well-known "Opfermoor" were also taken into account [55].

3. Materials and Methods

The Unstrut floodplain was surveyed by using electrical resistivity tomography (ERT), subsequent vibracore drillings, sedimentological multi-proxy analysis, and geochronological dating.

3.1. Electrical Resistivity Tomography (ERT)

Two-dimensional electrical resistivity tomography (ERT) measurements were conducted in order to obtain information on sedimentological patterns along a 624 m long transect comprising the southwestern hillslope to floodplain transition and almost the entire Unstrut floodplain (Figure 3). The transect also crosses the Unstrut itself, which is approx. 7 m wide and 0.9 m deep at this location. Measurements were carried out using the multi-electrode system RESECS (GeoServe Kiel) with standard electrodes stuck in the ground on land and a water electrode cable across the river bottom. A Wenner configuration was used with a 1 m spacing of the electrodes [56]. The longitudinal profile was processed by means of the inversion software pyGIMLI [57] using a triangular grid and explicitly taking into account the water body of the Unstrut. Three iterations were used to generate the 2D profile. The root mean square error (RMS) was 6.7%.

3.2. Drilling Campaigns

During initial project planning three drillings were arranged in the longitudinal river direction near the villages Bollstedt (Boll16), Seebach (See16), and Großengottern (Gro16), with coring distances of between two and three kilometres [58]. Based on this, an area between Seebach and Großengottern was surveyed during summer 2019 (Figure 1C). The investigated cross-section is southwest–northeast orientated and approx. 860 m long.

For vibracoring, an Atlas Copco Cobra Pro driving core device and 1 or 2 m long open coring systems with core diameters of 100 mm, 80 mm, and 60 mm were used. Drillings were carried out until assumed Pleistocene deposits were reached in order to guarantee recovering the entire Holocene sediment sequence. Macroscale features were subsequently described by following the German soil mapping instructions [59] and using Soil Colour Charts [60].

Three drilling cores were sampled for further laboratory treatment (Section 3.4). Coring site SG19_1a is located on the southwestern hillslope to floodplain transition. Core UA19_5a was drilled in the central Unstrut floodplain, approx. 70 m from the recent channel. Coring site UA19_8a is located in the northeastern Unstrut floodplain.

3.3. Positioning and Surface Levelling

A Topcon HiPer III GNSS system ensured precise positioning measurements. Satellite Positioning Service of the Federal Republic of Germany (SAPOS) was used to correct the measurements and guarantee positioning accuracy in the centimetre to millimetre range. Additionally, a LiDAR digital elevation model with 1 m and 5 m horizontal resolution was provided by the Free State of Thuringia (TLVermGeo).

3.4. Laboratory Methods

A total of 74 samples were taken for further laboratory treatment. Analyses were performed using the fine-earth fraction ($\leq$2.0 mm) of air-dried samples. The sediment colours were measured using a spectrophotometer (Konica Minolta CM-5) on sieved (<2000 µm), homogenized, and dried samples [61,62]. In this study L* values were used to indicate the extinction of light (0 = absolute black, to 100 = absolute white) [61,63].

Total carbon (TC) was measured on milled samples using an Elementar CN-analyser vario EL cube. $CaCO_3$ content was determined using an Eijkelkamp Scheibler calcimeter. Inorganic carbon content (TIC) was calculated by multiplying $CaCO_3$ by 0.12 [64,65]. It is important to mention that the deposits frequently contain mollusca fragments, which in some cases may lead to an overestimation of the TC and $CaCO_3$ content. Organic carbon content (TOC) was calculated by subtracting the TIC from the TC.

Particle size distribution was measured using a Laser Diffraction Particle Size Analyzer (Beckman Coulter LS 13 320). Organic matter was removed by treating the samples with 0.7 mL 15% hydrogen peroxide (H_2O_2) at 70 °C for several hours. Grain size measurement was not performed for one peat sample (UA19_5a, 4.7 to 4.9 m below the surface) because no representative sample remained after H_2O_2 treatment. To keep particles dispersed,

the samples were treated with 1.25 mL $Na_4P_2O_7$ (0.1 mol·L^{-1}) for 12 h on an overhead shaker [66,67]. The grain size distribution was determined by applying the Mie theory (Fluid RI: 1.33; Sample RI: 1.55; Imaginary RI: 0.1) [68].

The ΔGSD is the difference between grain size frequency calculated with the Fraunhofer approximation and grain size frequency calculated with the Mie theory [69]. As the complex refraction index (only considered by Mie) varies for different minerals, the ΔGSD indicates post-depositional enrichment of pedogenically formed minerals within the submicron GS fractions [69].

For numerical values, the deviations were additionally calculated for the grain size range 0.2 to 0.3 µm. Particles < 0.3 µm were predominantly formed in situ and particles >0.2 µm could be detected by laser diffraction. High ΔGSD values indicate the presence of post-depositional formed particles in this size fraction.

3.5. Numerical Dating

A total of 37 samples were taken for numerical dating to establish a chronological framework. Radiocarbon dating was carried out on 32 samples at the Curt-Engelhorn-Centre of Archaeometry (MAMS) and at Beta Analytic (BETA) using the Accelerator Mass Spectrometer (AMS) technique [70]. Dated material includes charcoal, plant fragments, wood, peat, and bulk organic sediments. Samples were pretreated using the acid-alkali-acid method [71]. Conventional ^{14}C ages (BP) were calibrated (2σ probability) in calendar years BP (cal BP) using the IntCal20 calibration set [72]. Uncalibrated radiocarbon dates taken from the literature were calibrated in the same way.

Additionally, five samples were taken for luminescence dating at site SG19_1a. Sample preparation and equivalent dose (De) measurements were conducted in the luminescence laboratory of the Department of Human Evolution (Max Planck Institute for evolutionary Anthropology) in Leipzig. For De measurements, the 4-11 µm quartz fraction was utilized and single aliquot regenerative dose (SAR) measurements were conducted on a Risoe TL/OSL DA 15 reader equipped with a calibrated $^{90}Sr/^{90}Y$ beta-source with a dose rate of approximately 0.03 Gy/s [73]. The quartz OSL signal was stimulated at 125 °C for 40 s using blue diodes and the 340 nm signal was detected through a Hoya U-340 filter. To create the dose response curve, four dose points were measured. Ten aliquots were used per sample to determine the De-mean value. Preheat and cutheat temperatures were set to 180 °C. This temperature combination allowed successful recovery of a dose with a measured to given dose ratio of 1.07 ± 0.02. The concentrations of radionuclides (activity of ^{238}U, ^{232}Th and ^{40}K) were determined using high resolution gamma spectrometry undertaken in the Felsenkeller laboratory of the VKTA in Dresden. An a-value of 0.035 ± 0.01 was used. The cosmic dose rate contribution was estimated by taking into account the geographical coordinates including height a.s.l. and the sampling depth.

4. Results

4.1. Electrical Resistivity Profiling

The ERT inversion model of the transect generally indicates horizontal layered deposits and only minor lateral changes (Figure 3). The upper approx. 1.5 m shows high resistivity values (40–100 Ωm), explained by the severe drought during summer 2019. Below this, a 4 to 6 m thick zone with considerable low resistivity values is observed (<20 Ωm). Within this zone, the lowest values (<10 Ωm) are located in the northeastern part of the transect, possibly caused by wetter environmental conditions in this specific area. Underneath (approx. 5 to 7 m below surface) the model shows an increase in electrical resistivity again with values up to 100 Ωm. This is related to coarse-grained deposits. Both the ground surface and this higher resistivity zone slightly decline towards NE.

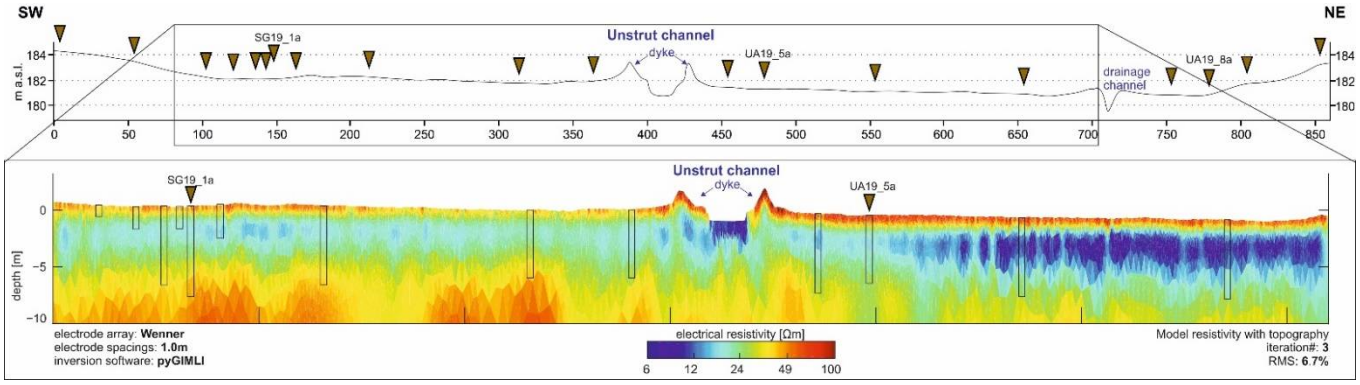

Figure 3. (**Top**) Exaggerated (approx. 5×) surface elevation profile of the surveyed cross-section in the upper Unstrut catchment (Figure 1C). Positions of investigated sites are indicated by red triangles. Named drillings were chosen for laboratory treatment. (**Bottom**). Results of ERT measurements with assumed depth of drillings.

4.2. Stratigraphic Results

The stratigraphic results from the investigated cross-section and initial floodplain drillings (Boll16, See16 and Gro16) are shown in Figures 4 and 5. Core photos and laboratory results of sampled drilling cores SG19_1a (southwestern hillslope to floodplain transition), UA19_8a (northeastern hillslope to floodplain transition), and UA19_5a (central floodplain) are shown in Figures 6–8 and are available as Supplementary Material (Table S1).

4.2.1. Hillslope Deposits

On both sites the Unstrut floodplain is bordered by gently inclined hillslopes in the area of the arranged cross-section (Figure 1C). The investigations reveal three stratigraphic hillslope units described in the following:

Gravelly to Sandy Sediments (Interpreted as Slope Debris)

At the southwestern slope (core SG19_1 and SG19_1a), gravelly to sandy sediments (interpreted as slope debris) were drilled in the lowermost parts. Gravels are poorly rounded to sharp-edged and can be assigned to the Triassic Keuper series. Grain size distribution from the sampled core SG19_1a (6.7 to 8.0 m) shows an increased proportion of the mS to cS fractions (Figure 6) and consequently a relatively high median GS of 329 µm. $CaCO_3$ content is extremely high (56.6%) whereas TOC is equal to zero. Luminance shows a maximum of approx. 74.0. At the southwestern slope (cores SG19_1 and SG19_1a), gravelly to sandy slope debris was drilled in the lowermost parts. Gravels are poorly rounded to sharp-edged and can be assigned to the Triassic Keuper series. Grain size distribution from the sampled core SG19_1a (6.7 to 8.0 m) shows an increased proportion of the mS to cS fractions (Figure 6) and consequently a relatively high median GS of 329 µm. $CaCO_3$ content is extremely high (56.6%) whereas TOC is equal to zero. Luminance shows a maximum of approx. 74.0.

At the northeastern section of the transect slope, deposits were recovered at drilling sites UA19_9 (>2.0 m) and UA19_8a. Field investigations from core UA19_9 indicate a heterogeneous texture ranging from sandy to clayey and increased stone content originating from local Keuper components. Grainsize data from the sampled core UA19_8a (5.08 to 5.6 m) are characterized by a silty to sandy texture (median GS: 22.6 µm), with embedded sandstone debris (5.1 to 5.3 m) clearly indicating lateral input from the adjacent hillslope (Figure 8). In this section $CaCO_3$ content (6.2%) and luminance values (61.1) are slightly increased, whereas the TOC content (0.8%) is rather low.

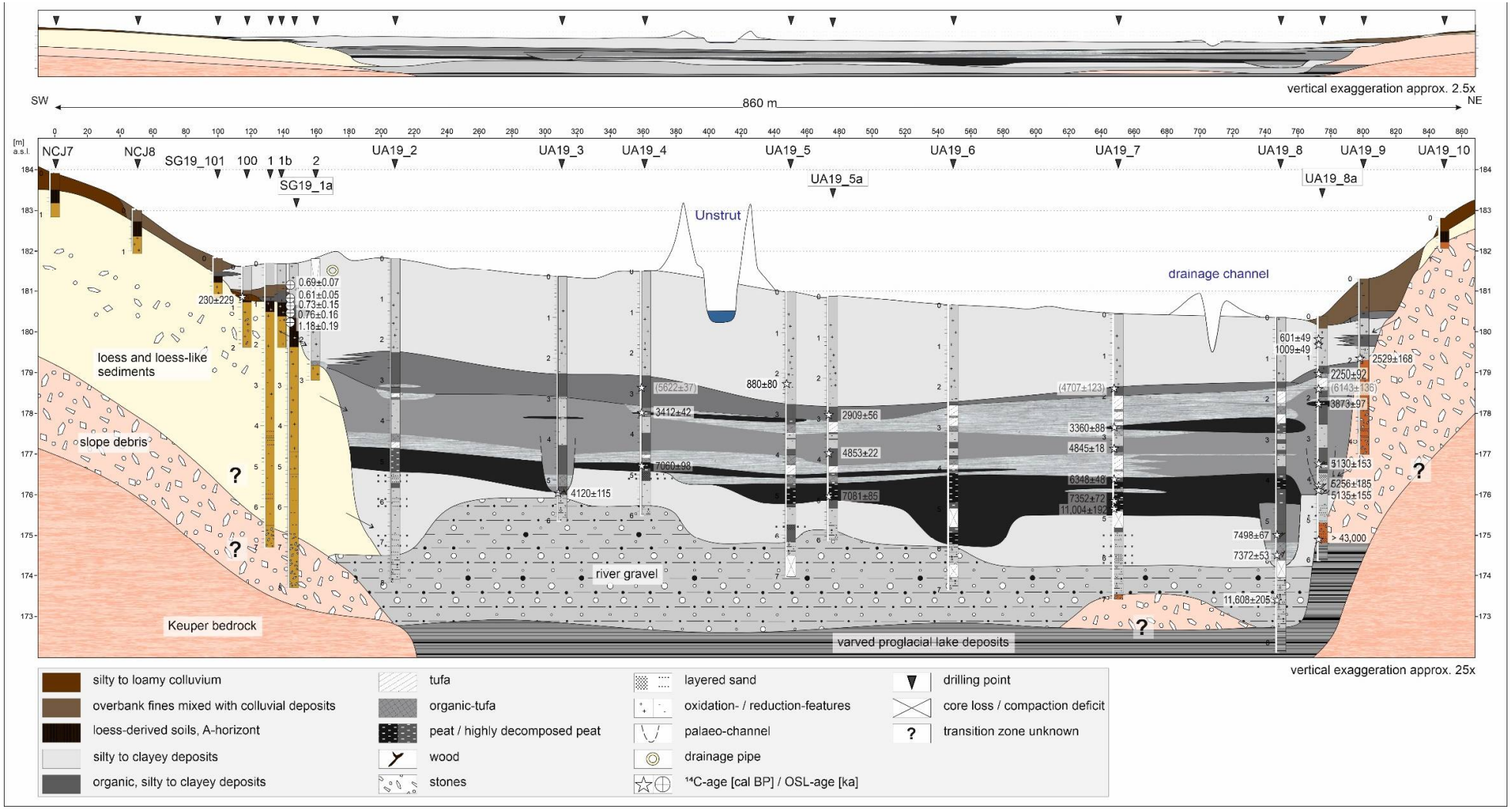

Figure 4. (**Top**) Valley cross-section exaggerated by the factor 2.5 for a more realistic impression of morphological conditions and sediment distribution. (**Bottom**) Valley cross-section exaggerated by the factor 25.

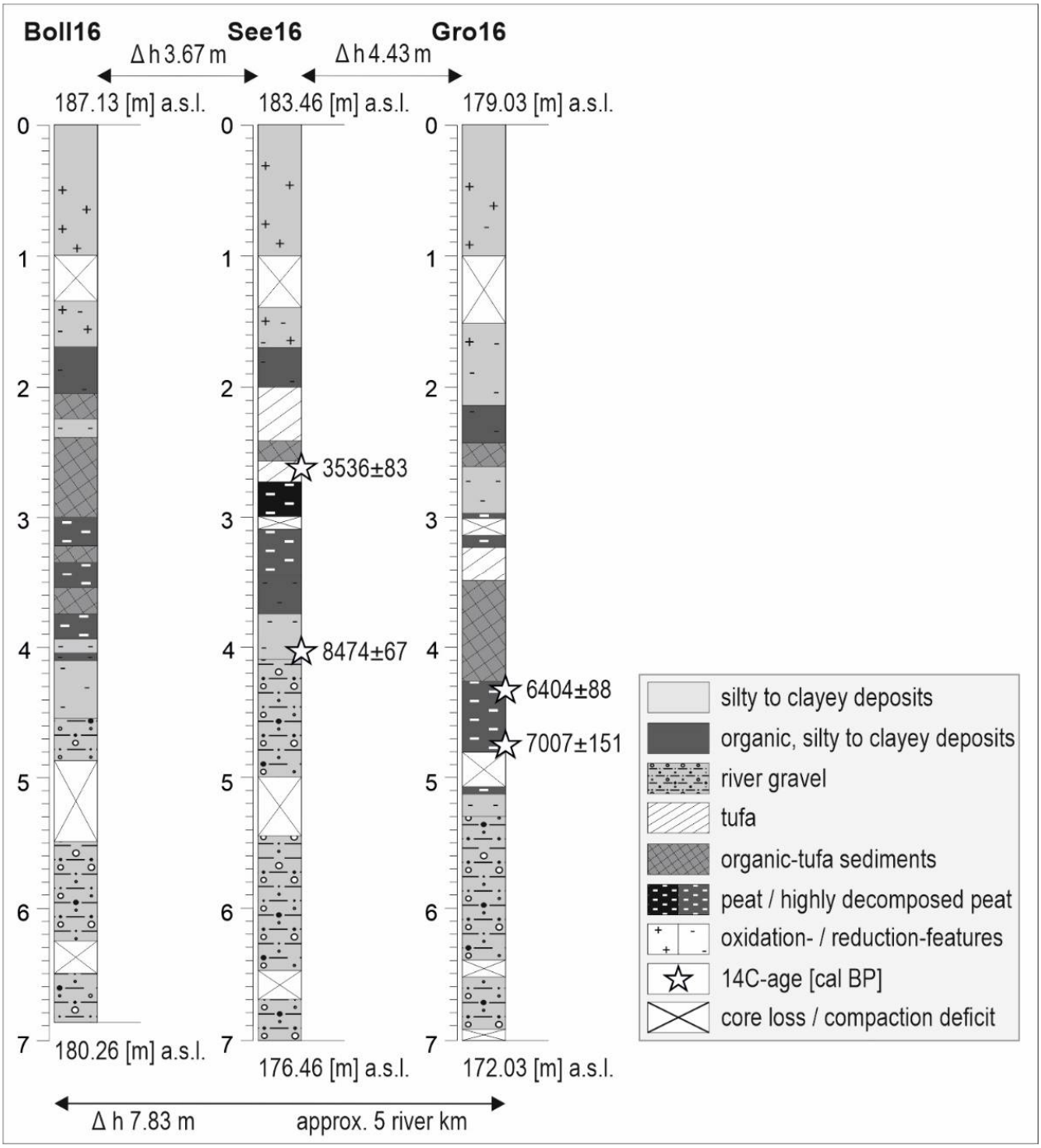

Figure 5. Drilling results from initial drillings Boll16, See16, and Gro16 (Figure 1C).

Predominantly Silty Sediments (Interpreted as Loess and Loess Derivate)

Silty sediments (interpreted as loess and modified-loess sediments) were surveyed at the investigated sites NCJ7, NCJ8, SG19_101, SG19_100, SG19_1, SG19_1b, SG19_1a, SG19_2, and UA19_10. The greatest thicknesses (approx. 5.0 m) were obtained on the southwestern slope (core SG19_1 and SG19_1a). In comparison, a considerably lower thickness of only 0.5 m was investigated at the northeastern hillslope (UA19_10), indicating a typical asymmetric loess deposition [34,74].

The sampled core SG19_1a reveals loess deposits between 1.4 and 6.7 m (Figure 6), with a gleyic Chernozem developed in the uppermost 0.6 m (1.4 to 2.0 m). Grain size data indicate a dominance of mSi and cSi fractions (median GS: 18 to 30 µm), a typical compo-

sition for Central European loess deposits [75]. However, thin intercalated reddish sand layers in the section between 5.5 and 6.7 m indicate reworking processes (e.g., solifluction) which are likely related to periglacial conditions during the latest Pleistocene [76,77]. (TOC content is low (0.2 to 0.4%) in the loess deposits (2.0 to 6.7 m) and the $CaCO_3$ content ranges between 10.7 and 17.9%. The achieved luminance is comparatively high (63.7 to 68.1). Samples from the gleyic Chernozem (1.4 to 2.0 m) show a stepwise decreasing median GS from the bottom to the top (32.3 to 13.7 µm) whereas the clay content increases upwards (11.0 to 20.4%). TOC content also increases upward from 1.2 to 1.8% and the $CaCO_3$ content ranges between 17.6 and 32.1% in this section. Luminance values are considerably reduced in the gleyic Chernozem, ranging between 53.5 and 59.2.

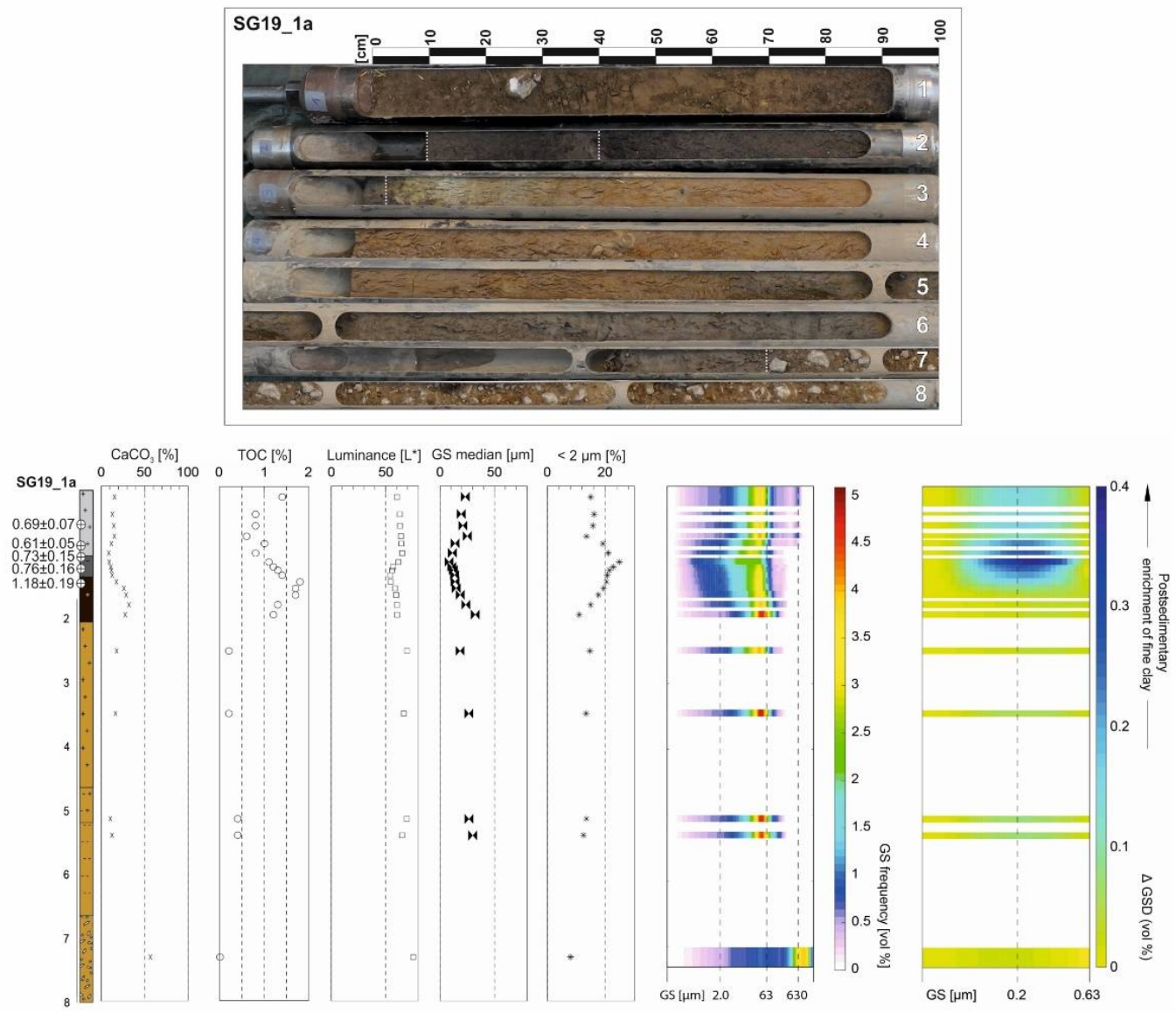

Figure 6. (**Top**) Drilling core SG19_1a showing gravelly to sandy slope debris (6.7 to 8.0 m) covered by loess and loess-like sediments (1.4 to 6.7 m), with a developed gleyic Chernozem between 1.4 and 2.0 m. Above (<1.4 m) overbank fines were drilled which are influenced by ploughing in the uppermost 0.3 m. (**Bottom**) Laboratory results obtained for drilling core SG19_1a. The schematic illustration (left of the graphs) refers to Figure 4.

On the northeastern slope, field investigations of core UA19_10 indicate a loamier-textured loess derivate than in core SG19_1a. This might be explained by the heterogeneously textured geological substrate below which may have been incorporated during reworking processes. A 0.35 m thick humic A-horizon was recovered in the upper parts of the loess deposits.

Silty and Sandy Sediments (Interpreted as Colluvial Deposits)

Loess deposits are covered by shallow hillslope colluvium (<1 m). Colluvium was encountered at the investigated sites NCJ7 (southwest slope) and UA19_10 (northeast slope), elevated two to three metres above the recent floodplain surface (Figure 4). Here, colluvial layers appear a dark brown colour. Field description at NCJ7 indicates a non-gravelly, silty texture and medium to high $CaCO_3$ content (approx. 10%). In contrast, field investigation reveals the texture is sandy loam at site UA19_10, with embedded stones, pottery, and charcoal suggesting human-induced soil erosion.

However, especially at the transition to the floodplain (NCJ7, SG19_101, UA19_8a, and UA19_9), clear separation from the uppermost floodplain sediments is hardly possible, as constant ploughing has resulted in substrate mixing in these specific areas. Here the mixed colluvium is usually somewhat lighter, has a crumbly structure and contains a clearly visible proportion of small mollusca shells. The sampled core UA19_8a contains such colluvium in the uppermost approx. 0.35 m (Figure 8). Grain size measurements indicate loamy silt (median GS: 9.2 µm) with maxima in the fSi to cSi fractions. The ΔGSD value is noticeably high (1.5%), TOC content is slightly increased (2.3%), and $CaCO_3$ content is rather moderate (11.7%).

4.2.2. Varved Silty and Sandy Sediments (Interpreted as Proglacial Lake Deposits)

At the northeastern edge of the Unstrut floodplain (UA19_8 and UA19_8a), varved silty and sandy sediments were drilled in the lowermost core sections. They show a fine alternation of grey silty to sandy and dark clayey to silty layers, which become irregular towards the upper boundary (Figure 8). In light of regional stratigraphic knowledge on Quaternary valley fillings [48], we interpreted these deposits as proglacial lake sediments which existed in front of retreated ice sheets during Elsterian glacial cycles (MIS 12). Accordingly, it can be assumed that the entire recent valley floor was formerly covered by laminated lake sediments. Core UA19_8a reveals an upper boundary around 174.8 m a.s.l. (5.6 m below surface), whereas core UA19_8 shows varved deposits below approx. 172.8 m a.s.l. (7.6 m below surface). The height difference of the upper boundary (approx. 2.0 m) indicates subsequent erosion of the varved deposits. The underlying bedrock was never reached at one of the drillings, so that total thickness of the varved deposits remains unclear. However, assuming typical horizontal lacustrine layering, these two drillings indicate former thicknesses of at least 2.5 m.

4.2.3. Fluvial Deposits

Core drillings in the Unstrut floodplain reveal four types of fluvial deposits described in the following.

Matrix-Supported Gravels (Interpreted as Fluvial Bedload Deposits)

Gravels embedded in a fine-grained sediment matrix were encountered in the lowermost sections of the cores UA19_2, UA19_3, UA19_4, UA19_5, UA19_5a, UA19_6, UA19_7, and UA19_8 (Figure 4) and confirmed by the initial drillings Boll16, See16, and Gro16 (Figure 5). These sediments are interpreted as fluvial bedload deposits. Gravel layers frequently show a fining-upwards tendency, with an increased matrix content in the upper parts. Roundness of the gravels varies from well-rounded to subangular. Petrographically the gravels are consistent with the local geology and are mainly classified as lime-, mud-, sand- and siltstone gravels. At the drilled cross-section the upper boundary ranges between approx. 175.8 m a.s.l. (core UA19_3) and 174.0 m a.s.l. (UA19_8), with declining heights

towards the NE. At drilling sites UA19_7 and UA19_8, gravel thicknesses of only 0.8 and 1.5 m were investigated. The sampled core AM19_5a shows gravelly deposits between 5.7 and 6.0 m (Figure 7). Grain size results from the surrounding matrix reveal a silty (>40%) to sandy (>50%) texture and a relatively coarse median GS of 69.9 µm. TOC content is low (0.6%) whereas $CaCO_3$ (45.4%) and luminance (67.1) data show high values.

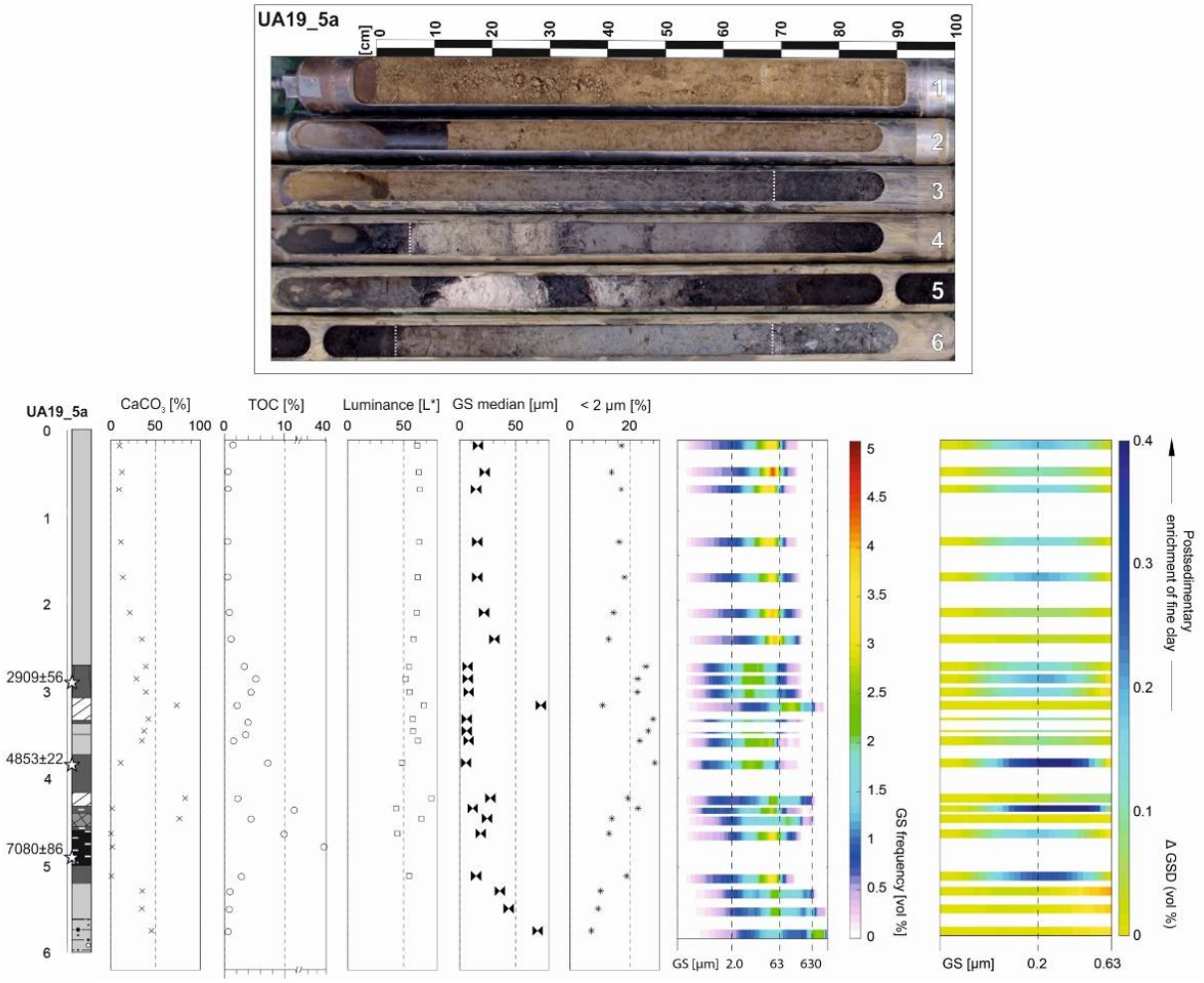

Figure 7. (**Top**) Drilling core UA19_5a showing matrix-supported gravels (>5.7 m) covered by basal overbank fines (5.05 to 5.7 m). From 3.1 to 5.05 m "rieth series" deposits with interbedded overbank fines (3.3 to 4.1 m) were drilled. Between 2.7 and 3.1 m humic overbank fines were recovered, changing to homogeneous yellowish brown to greyish brown overbank fines in the uppermost 2.7 m. (**Bottom**) Laboratory results obtained for drilling core UA19_5a. The schematic illustration (left of the graphs) refers to Figure 4.

Peat and Tufa Deposits ("Rieth Series" Deposits)

Peat and tufa deposits were drilled in almost all floodplain cores; both belong to the aforementioned "rieth series" [48]. The "rieth series" show the largest thicknesses (>3.0 m) in the northeastern part of the cross-section (Figure 4) as well as at initial drilling Gro16 (Figure 5). In contrast, "rieth series" deposits are less well-preserved or absent at the transitional zone from the Unstrut floodplain to the adjacent hillslopes (SG19_100, SG19_1, SG19_1a, SG19_1b, UA19_8a, and UA19_9).

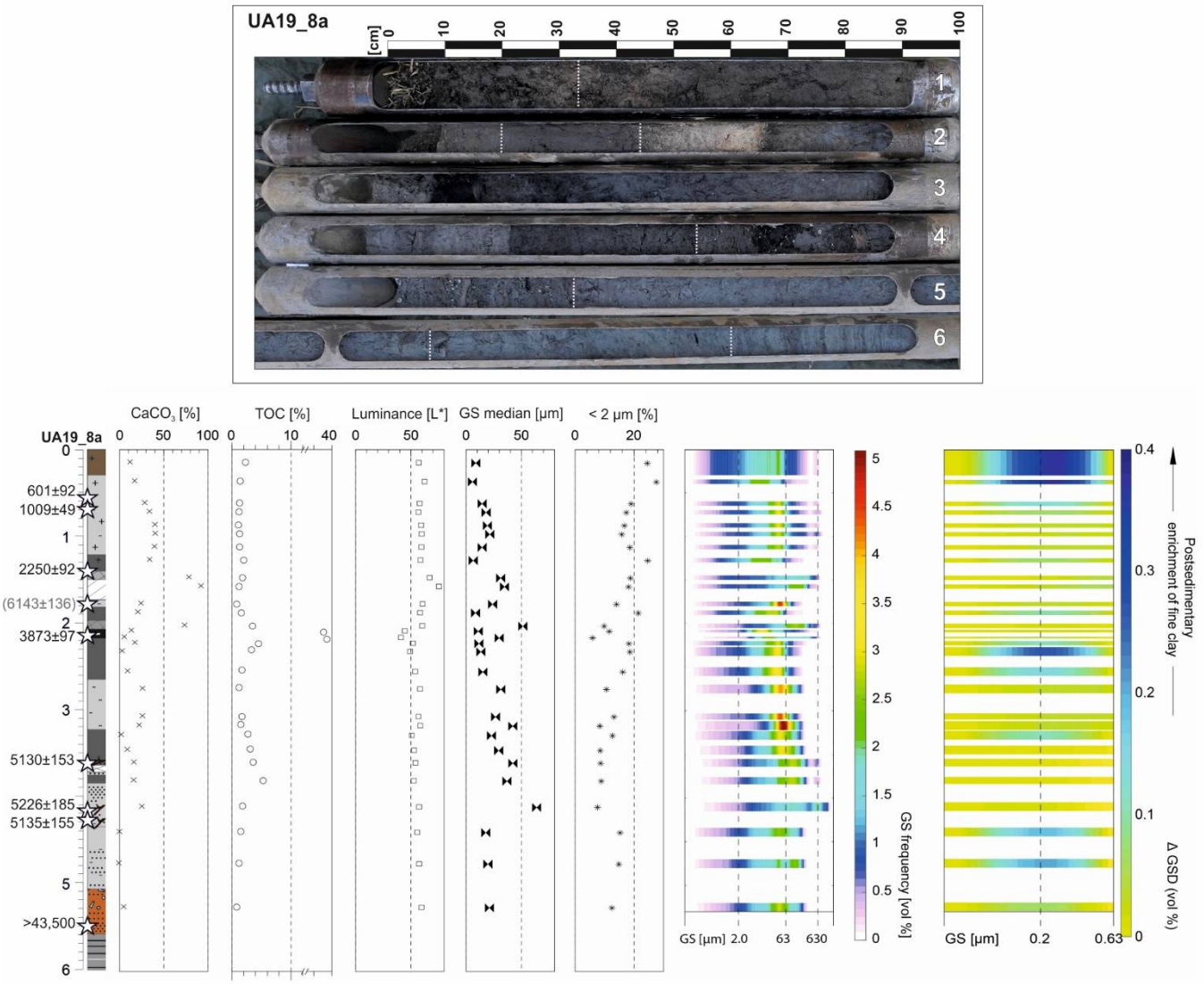

Figure 8. (**Top**) Drilling core UA19_8a shows laminated lake sediments below approx. 5.6 m, covered by fine-grained slope debris (5.08 to 5.6 m). Basal overbank fines were drilled from 4.33 m to 5.08 m overlain by paleochannel infillings (3.55 to 4.33 m) and overbank fines intercalated in "rieth series" deposits (1.45 to 3.55 m). Above this (1.2 to 1.45 m), organic overbank fines were recovered changing upwards to greyish brown overbank fines. The uppermost 0.35 m consists of mixed colluvium with overbank fines. (**Bottom**) Laboratory results obtained for drilling core UA19_8a. The schematic illustration (left of the graphs) refers to Figure 4.

Peat characteristics: Peat was drilled in the cross-section cores UA19_2, UA19_3, UA19_4, UA19_5, UA19_5a, UA19_6, UA19_7, UA19_8, and UA19_8a, as well as at initial drilling sites Boll16, See16, and Gro16 (Figures 4 and 5). Peat layers show different stages of decomposition but usually occur as highly decomposed peat. Generally, the peaty deposits appear a black to dark brown colour. They are interspersed by mollusca fragments, fine roots, and more or less decomposed reed leaves. The greatest peat thicknesses (approx. 2.0 m) were achieved in the lower section of the "rieth series", around 4.0 to 4.5 m below the floodplain surface. In contrast, peat deposits are comparatively thin in the upper parts of the "rieth series" as well as at the floodplain to hillslope transition (e.g., UA19_3, UA19_4, UA19_7, and UA19_8a). Overall, peat deposits from the sampled cores UA19_5a and UA19_8a show low luminance (41.5 to 44.9) and high TOC content (6.7 to 37.7%), already indicated by their dark colour (Figures 7 and 8). The basal peat layer from core UA19_5a (4.75 to 5.05 m) is characterized by a maximum TOC content of 37.7%, decreasing to 9.9%

(4.6 to 4.7 m) and 11.6% (4.33 to 4.4 m) in the highly decomposed peat strata above. The peat layer from core UA19_8a (2.07 to 2.17 m) again shows high TOC values (30.9 and 34.9%). $CaCO_3$ content of peat deposits is very low to low (0.3 to 1.7%) for core UA19_5a, thus confirming the field classification [59]. In contrast, core UA19_8a has a maximum of 13.8% $CaCO_3$ (2.07 to 2.17 m), which can be attributed to the smallest intercalated mollusca fragments, since field classification indicates rather low $CaCO_3$ content. Grain size measurements achieved for peat layers at core UA19_5a (4.3 to 4.4 m and 4.6 to 4.7 m) reveal median GS of between 11.7 µm and 18.9 µm with maxima in the mSi to cSi fractions. ΔGSD is increased (2.2%) in the peat sample from 4.3 to 4.4 m. The lowest peat sample from core UA19_8a (2.15 to 2.17 m) is coarser with a median of 30.5 µm and maxima in the mSi (25.9%) and fS fractions (20.7%).

Tufa characteristics: Tufa deposits appear bright white to light yellow in colour, changing to grey in sections with increased TOC content. They often overlie the peaty deposits or are intercalated with them. Tufa deposits are highly porous, often sandy, and frequently contain mollusca fragments as well as lime tubes. Laboratory results for tufa samples from cores UA19_5a and UA19_8a reveal extremely high $CaCO_3$ content (73.6 to 92.7%). The TOC content ranges between 1.2 and 5.9% and luminance is correspondingly high (58.3 to 76.0). The median GS distribution does not show a clear trend and ranges between 6.4 and 72.8 µm (Figures 7 and 8).

Predominantly Silty Sediments (Interpreted as Overbank Floodplain Deposits)

Silt-dominated sediments are preserved in various stratigraphic positions within the Unstrut floodplain. They are interpreted as overbank fines. Based on the stratigraphic position and distinctive sediment properties, four different types of overbank fines can be distinguished: (I) basal overbank fines, (II) overbank fines intercalated with peat and tufa ("rieth series"), (III) organic overbank fines covering peat and tufa ("rieth series"), and (IV) the uppermost overbank fines.

(I) Basal overbank fines

Silt-dominated overbank fines with several intercalated, thin sand layers were almost ubiquitously drilled above the matrix-supported gravels In the higher section, they are frequently bordered by basal peat layers of the "rieth series" Thicknesses of up to two metres were drilled (UA19_2, Figure 4). However, at the sites UA19_ 3, UA19_8 thicknesses are lower, which might be related to post-depositional river incision and related sediment mobilization. The overbank deposits exhibit a greyish to greenish colour with severe reduction features; in some cases they are interspersed by fibrous plant fragments.

At drilling UA19_5a, basal overbank fines were recovered between 5.05 and 5.7 m below the surface (Figure 7). Grain size results from three samples indicate a silty to clayey sediment texture, with a striking fining-upwards trend. This is expressed by the median GS which decreases upwards from 44 µm (5.45 to 5.55 m) to 35.9 µm (5.25 to 5.35 m) and subsequently to 14.8 µm (5.08 to 5.18 m). Similarly, a gradual upwards trend is observable for the clay fraction (<2 µm), increasing from 9.5 to 10.3% before reaching 19.0%. An interesting observation is the noticeably high ΔGSD value (1.1%) in the uppermost sample (5.08 to 5.18 m). $CaCO_3$ content reduces upwards from approx. 35% (5.45 to 5.55 m and 5.25 to 5.35 m) to 0.6% (5.08 to 5.18 m). The same trend holds true for luminance, declining upwards from 68.4 to 66.2 and subsequently to 55. In contrast, TOC content slightly rises upwards from 0.8% (5.45 to 5.55 m) to 0.9% (5.25 to 5.35 m) followed by a distinct TOC increase (2.8%) in the upper part (5.08 to 5.18 m).

Core UA19_8a shows basal overbank fines on top of slope debris (4.33 to 5.08 m). Two samples from this section once again indicate a silt-dominated texture (median GS: 19.2 and 21.1 µm) with intercalated sand layers. The ΔGSD values are slightly increased (0.6 to 0.8%), $CaCO_3$ content is low (0.5 and 1.1%), and the TOC content slightly increases upwards in this section (1.2 to 1.5%). Luminance values drop upwards slightly from 58.8 to 56.9.

(II) Overbank fines intercalated with peat and tufa ("rieth series")

Overbank fines are irregularly interfingered with peat and tufa deposits of the "rieth series". The deposits show a grey to very dark grey colour with distinct reduction features. The sampled core UA19_5a shows corresponding overbank fines from approx. 3.3 to 4.1 m below the surface (Figure 7). Here, grain size results reveal a rather small median GS (5.8 to 8.1 µm) with maxima in the fSi to mSi fractions, and a noticeably increased clay content (23.4 to 28.4%). The increased ΔGSD value (1.7%) in the lowermost section (3.8 to 3.9 m) of the overbank fines is very obvious. TOC content is increased (3.9%, 3.5% and 7.2%) in the upper (3.34 to 3.37 m and 3.48 to 3.5 m) and especially in the lower section (3.8 to 3.9 m), whereas only 1.5% was measured for the middle part (3.55 to 3.65 m). $CaCO_3$ data show a clearly discernible trend of increasing values upwards, from 11.0 to 42.0%. In this context, small intercalated mollusca fragments as well as tufa deposits drilled above may have influenced the measurements in the upper sections, since field classification indicates rather low $CaCO_3$ contents here. Luminance ranges between 48.7 (3.8 to 3.9 m) and 62.9 (3.55 to 3.65 m). UA19_8a shows mainly silty overbank fines (silt content: 62.5 to 75.9%) between 2.2 and 3.55 m, with an increased ΔGSD value (1.0%) between 2.27 and 2.37 m. In this section, TOC content ranges between 1.2 and 4.5% with a maximum (3.3 and 4.5%) in the uppermost part (2.2 to 2.37 m). $CaCO_3$ content ranges between 2.6 and 26.7% while luminance ranges between 49.9 and 59.4.

(III) Organic overbank fines covering peat and tufa ("rieth series")

Approx. 0.1 to 1.0 m thick dark overbank fines cover peat and tufa of the "rieth series". A greater thickness was obtained in the southwestern part of the transect (cores UA19_2, UA19_3 and UA19_4), thinning out towards NE. Characteristics are finely distributed mollusca shell fragments resulting in a carbonate-rich field classification of the sediment matrix [59]. The sampled core UA19_5a reveals organic overbank fines from 2.7 to 3.1 m below the surface (Figure 7). The median GS is comparatively small (7.0 and 8.2 µm) and especially striking are the increased clay content (22.7 and 25.5%) and the increased ΔGSD (~0.8%). TOC content ranges between 3.3 and 5.2% and luminance shows values from 51.9 to 55.3. The $CaCO_3$ content is relatively high (28.7 and 39.3%) but measurements might be influenced by the smallest mollusca fragments. At sampled core UA19_8a, organic overbank fines were recovered on top of organic tufa deposits, from approx. 1.2 to 1.45 m below the surface (Figure 8). Similarly to core UA19_5a, median GS is rather small (7.2 µm) with a strikingly high clay content (24.7%). TOC content is 2.0% and luminance 59.1. $CaCO_3$ content is relatively high (34.3%).

(IV) Uppermost overbank fines

Up to 2.7 m (cores UA19_5 and UA19_5a), overbank fines were encountered in the uppermost parts of the Unstrut floodplain. In general, they appear a relatively homogeneous yellowish brown to brown colour in the upper part, discernibly changing to greyish brown downwards. Below approx. 1.0 m, hydromorphic features (e.g., iron and manganese concretions, rust stains) become frequent, which is related to anoxic conditions in the corresponding sections. The uppermost approx. 0.4 m are influenced by recent ploughing. At sampled core UA19_5a, uppermost overbank fines were drilled to a depth of 2.7 m (Figure 7). Grain size distribution shows a dominance of the mSi to cSi fractions. Between 2.7 and 0.7 m, there is a stepwise decrease in median GS upwards from 31.1 to 14.9 µm. Above this the sediment texture is in the same range (median GS: 22.5 and 16.6 µm). Slightly higher ΔGSD values (up to 0.8%) are evident for the uppermost 1.8 m. The TOC content is generally low (0.5 to 1.1%), but slightly increases (1.4%) in the ploughing zone (<0.4 m). The $CaCO_3$ content ranges between 9.3 and 34.7%, generally increasing with depth. Luminance shows only minor variations (58.8 to 64.5), slightly decreasing with depth. The sampled core UA19_8a is characterized by overbank fines from 0.35 to 1.2 m (Figure 8). Overall, the sediment properties are very similar to the overbank fines from core UA19_5a. Grain size measurements indicate a dominance of the mSi to cSi fractions (median GS: 6.3. to 21.9 µm) again. However, it is striking that the mS content is slightly increased (3.5 to 7.5%).

A noticeably high ΔGSD value (1.5%) is evident in the uppermost section (0.35 to 0.4 m). TOC content ranges from 1.1 to 1.4%, $CaCO_3$ content is relatively high (16.9 to 40.5%) and luminance varies only slightly (57.1 to 62.5). At sampled drilling SG19_1a, overbank fines were encountered in the uppermost 1.4 m below the surface (Figure 6). Median GS ranges from 8.2 to 24.9 µm, with dominance in the mSi to cSi fractions. From 1.4 to 1.1 m, clay content increases upwards stepwise from 20.6 to 24.8%. Increased mS content (2.3% to 6.0%) is obvious in the uppermost 0.9 m. ΔGSD is increased in the uppermost overbank fines (0.6 to 1.5%) with a maximum around 1.1 m below the surface. TOC is generally on a low level again (0.6 to 1.4%), but slightly higher (1.4%) in the lower part of the overbank fines (1.1 to 1.4 m) and in the uppermost ploughing horizon (<0.3 m). $CaCO_3$ content ranges from 8.9 to 15.3% and is therefore lower than at coring sites UA19_5a and UA19_8a. Luminance shows values between 53.3 and 63.8.

Paleochannel Deposits

Paleochannels are a typical element of fluvial architecture [78,79] and a well-known feature of Central European river systems [30]. Three infilled paleochannel structures were detected by the drilling program, mainly inferred from comparison with neighbouring drilling cores and larger differences to the established sediment chronostratigraphy (Figure 4). UA19_3 shows some organic-rich sandy deposits (5.16 to 5.42 m) with larger plant fragments and wood above the common basal gravels. Above this (4.86 to 5.16 m), organic tufa deposits with mollusca fragments and plant remains were recovered, overlain by silty deposits. Commonly preserved basal overbank fines and thicker peat layers, which were instantly recovered in the neighbouring cores UA19_2 and UA19_4, are absent; furthermore, the aforementioned organic tufa deposits are deeper. Similarly, core UA19_8 shows organic tufa covered by silty deposits interspersed with larger mollusca fragments, plant remains, and wood between around 4.2 and 6.0 m. Once again, the commonly preserved basal overbank fines are missing here and instead gravels were drilled below. Peaty deposits cover the filled-up paleochannel. The sampled core UA19_8a shows paleochannel fillings on top of basal overbank fines (3.55 to 4.33 m). The paleochannel infillings have a strikingly higher sand content (36.5 to 50.5%, median GS: 37.9 to 64.5 µm) as well as markedly increased wood and mollusca fragments (Figure 8). TOC ranges between 1.8 and 5.3% and $CaCO_3$ content is increased (17.0 to 26.4%). Luminance shows values between 53.5 and 58.6.

4.3. Chronological Results

4.3.1. Radiocarbon Dating

The ^{14}C results are summarized in Table 1 and added to Figures 4–8. They cover the time span from the latest Pleistocene (11,608 ± 206 cal BP) until the late Holocene (230 ± 229 cal BP). Three ages show substantial inversions (UA 19_4: 280 to 290 cm; UA 19_7: 175 to 185 cm; UA 19_8a: 178 cm) which might be caused e.g., by pre-aged organic carbon or substantial old-wood effects [80,81]. One sample (UA19_8a: 550 cm) exceeds the ^{14}C dating limit (>43,500 BP). However, the remaining 28 ^{14}C ages are in chronological order and consistent.

4.3.2. Luminescence Dating

The luminescence properties of the fine-grain quartz signal allowed successful OSL dating. The results are summarized in Table 2 and are in chronological order, taking into account methodological error. For the uppermost part of a gleyic Chernozem from core SG19_1a (1.45 to 1.5 m below the surface), an OSL age of 1.18 ± 0.19 ka was detected. However, this age does not correspond to the Chernozem formation period and rather indicates the input of younger deposits or the bleaching of the uppermost parts of the Chernozem, maybe due to surface ploughing or bioturbation. Four calculated quartz OSL ages from the uppermost overbank fines range between 0.76 ± 0.16 and 0.61 ± 0.05 ka.

Table 1. Results of radiocarbon dating.

Site	Depth (cm)	Lab. No.	Material	^{14C} Age BP	Cal ^{14}C Age BP (2σ)	δ^{13}C (‰)
SG19-100	70–75	MAMS 51797	Charcoal	224 ± 19	230 ± 229	−28.6
UA19_3	537	MAMS 46836	Plant fragment	3766 ± 22	4120 ± 115	−25.4
UA19_4	280–290	MAMS 50031 *	Sediment	4891 ± 24	5622 ± 37	−13.0
UA19_4	345–352	MAMS 46828	Sediment	3192 ± 25	3412 ± 42	−28.6
UA19_4	474–482	MAMS 46829	Sediment	6153 ± 24	7060 ± 98	−23.3
UA19_5	225	MAMS 46824	Charcoal	1003 ± 23	880 ± 80	−23.9
UA19_5a	285–295	MAMS 50032	Sediment	2811 ± 21	2909 ± 56	−23.7
UA19_5a	380–390	MAMS 46830	Sediment	4292 ± 22	4853 ± 22	−20.1
UA19_5a	470–500	MAMS 46831	Peat	6189 ± 25	7081 ± 85	−27.3
UA19_7	175–185	MAMS 50030 *	Sediment	4165 ± 22	4707 ± 123	−12.6
UA19_7	272–278	MAMS 46832	Peat	3153 ± 27	3360 ± 88	−55.4
UA19_7	325–335	MAMS 50029	Sediment	4269 ± 22	4845 ± 18	−29.1
UA19_7	402–407	MAMS 46833	Peat	5555 ± 23	6348 ± 48	−25.8
UA19_7	458–462	MAMS 50028	Peat	6427 ± 25	7352 ± 72	−26.0
UA19_7	475–482	MAMS 46834	Peat	9667 ± 29	11,004 ± 192	−21.9
UA19_8	535	MAMS 46837	Wood	6593 ± 25	7498 ± 67	−28.6
UA19_8	587	MAMS 46838	Wood	6450 ± 25	7372 ± 53	−30.5
UA19_8	694	MAMS 46839	Plant fragment	10,079 ± 30	11,608 ± 205	−30.8
UA19_8a	55	MAMS 51798	Charcoal	614 ± 20	601 ± 49	−24.0
UA19_8a	67	MAMS 51799	Charcoal	1111 ± 20	1009 ± 49	−27.0
UA19_8a	140	MAMS 46825	Charcoal	2257 ± 25	2250 ± 92	−17.9
UA19_8a	178	MAMS 46826 *	Charcoal	5368 ± 30	6143 ± 136	−20.8
UA19_8a	215–217	MAMS 46835	Peat	3576 ± 22	3873 ± 97	−23.0
UA19_8a	363	MAMS 46840	Plant fragment	4467 ± 22	5130 ± 153	−23.4
UA19_8a	418	MAMS 46841	plant fragment	4578 ± 22	5256 ± 185	−21.6
UA19_8a	427	BETA 624727	Wood	4480 ± 30	5135 ± 155	−26.9
UA19_8a	550	BETA 624725	Charcoal	>43,500		−24.8
UA19_9	195	MAMS 46827	Charcoal	2440 ±20	2529 ± 168	−21.4
See16	259–273	BETA 457185	Plant material	3310 ± 30	3536 ± 83	−26.0
See16	404–409	BETA 457182	Plant material	7680 ± 30	8474 ± 67	−26.4
Gro16	430	BETA 457184	Plant material	5640 ± 30	6404 ± 88	−25.6
Gro16	470–480	BETA 457183	Plant material	6100 ± 30	7007 ± 151	−26.2

* Not included in the discussion due to obvious age inversions.

Table 2. Results of OSL dating.

Site	Depth (cm)	Lab. No.	Dose Rate (mGy/a)	Equivalent Dose (Gy)	Age (ka)
SG19_1a	55–61	L-Eva 1955	3.13 ± 0.18	2.15 ± 0.20	0.69 ± 0.07
SG19_1a	84–90	L-Eva 1956	3.48 ± 0.20	2.12 ± 0.10	0.61 ± 0.05
SG19_1a	102–108	L-Eva 1957	3.62 ± 0.21	2.64 ± 0.52	0.73 ± 0.15
SG19_1a	120–126	L-Eva 1958	3.29 ± 0.18	2.49 ± 0.50	0.76 ± 0.16
SG19_1a	145–150	L-Eva 1959	2.83 ± 0.14	3.33 ± 0.50	1.18 ± 0.19

5. Discussion

5.1. Floodplain Evolution

Based on an applied multi-proxy research program, fluvial sediment patterns in the upper Unstrut catchment were investigated. Except for three infilled paleochannels indicating lateral channel changes, relatively continuous sediment stratigraphy and robust chronological information allow detailed insights on the latest Pleistocene and Holocene floodplain evolution at the climatic transitional zone. In the following, fluvial development is discussed in selected time slices with the aim of evaluating the impacts of natural environmental and anthropogenic changes on floodplain evolution.

5.1.1. Younger Dryas to Preboreal Gravel Deposition

In the upper Unstrut valley, matrix-supported gravels were encountered in the lowermost section. The ERT results indicate that these coarse-grained deposits are preserved in the entire floodplain without major changes (Figure 3). Suitable material for ^{14}C dating is very rare and was recovered at drilling site UA19_8 only. Here, a plant fragment was dated as 11,608 ± 205 cal BP, indicating deposition during the late Younger Dryas to early Preboreal period [82,83]. From a geomorphic perspective, our results suggest less protective vegetation cover, enhanced sediment mobilization, and finally the bedload deposition of matrix-supported gravels in a braided river system with high runoff rates at the Pleistocene to Holocene transition [79,84,85]. This observation is in line with results from the Weser, Werra, or Wetterau catchment that report similar gravel deposition during the Younger Dryas to Preboreal period [23,86,87].

Shifts towards more negative $\delta^{18}O$ and $\delta^{13}C$ isotope values [88], a decrease in the $\delta^{13}C$ values [89] and changes in vegetation pattern from mainly steppe vegetation to Pinus and Betula forests [87,90,91], concordantly indicate a climate shift in the region from periglacial to warmer and wetter conditions at the Younger Dryas–Preboreal transition. The temporal coincidence with fluvial gravel aggradation in the Unstrut valley strongly indicates a causal relationship between increased fluvial activity and the corresponding environmental changes in this period. This is even more likely since other potential triggers of the fluvial system (e.g., human impact, tectonics, sea level changes) can be ruled out for this period in this region.

5.1.2. Preboreal to Early Atlantic Overbank Deposition and Soil Formation

Silty overbank fines cover the latest Pleistocene to early Holocene gravels. Most of the determined sediment properties of the overbank fines (e.g., median GS, $CaCO_3$, and TOC) show great similarity to those of the surrounding loess deposits (Figure 6), indicating that the majority of the overbank fines originate from soil erosion in the surrounding loess area. Sediment deposition seems to be related to vertical accretion of a well-defined channel, probably a meandering river pattern [92], and therefore indicates changes in the channel pattern of the Unstrut since the Younger Dryas–Preboreal braided channel situation. Sandwich dating with ^{14}C samples taken from the basal gravels (UA19_8) and covering peat layers (UA19_4, UA19_5a, UA19_7 and Gro16), one ^{14}C age from the corresponding overbank fines at core See16 as well as two basal ^{14}C ages from an incised paleochannel (UA19_8), date the silty overbank aggradation to the period between around 11.6 and 7.0 cal ka BP (Preboreal to early Atlantic period).

Whereas most of western and Central European floodplain studies assume rather stable floodplain conditions during this period, as expressed by limited floodplain aggradation, pedogenesis or peat formation [10–12,17], only a few studies describe early Holocene overbank deposition [22,32,93]. A question which needs to be discussed in this context relates to the triggering causes that result in erosion-prone surfaces, which are required to explain the observed Preboreal to early Atlantic overbank deposition [84]. Some studies discuss local environmental disturbances by Mesolithic hunters and gatherers [94–96]. However, since archaeological remains of Palaeolithic and Mesolithic communities are very rare in the intensively studied upper Unstrut area (Figure 2A) [50], their influence on sediment dynamics are rated as rather low here.

In addition to this anthropogenically driven explanation, natural causes might be responsible for an increased sediment supply. In this context, above-average early Holocene (11.5 to 8.5 cal ka BP) fire activity in the Central European Lowlands [96] potentially resulted in erosion-prone soil surfaces. However, since the investigated Preboreal to early Atlantic overbank fines generally lack macroscopic charcoal, no evidence for this natural fire model is provided by this study. Moreover, while erosion under closed forest cover may lead to substantial natural overbank fine deposition especially in larger catchments [29], the surveyed upper Unstrut floodplain is located in an upstream region (<700 km^2), so this explanation is not fully convincing here; this is particularly the case considering the almost

area-wide preservation of Preboreal to early Atlantic silty overbank fines in the relatively wide Unstrut floodplain.

So far, the most plausible explanation for the observed overbank deposition in the upper Unstrut valley concerns climate changes at the Pleistocene–Holocene transition and during the early Holocene [97,98] and a delayed reaction of the protective vegetation to these changes [99]. This may have temporarily resulted in soils being at least partly exposed during sudden climate changes, subsequently triggering soil erosion [100] and enhanced sediment input into the Unstrut floodplain. Soil erosion may have continued until re-established closed vegetation cover fully stabilized the surrounding slopes again. Evidence for corresponding early Holocene climate variabilities in the Unstrut catchment comes from regional paleoclimate studies. A short-lived climate deterioration to drier and/or colder conditions shortly before 11.0 ka BP (bond event 8, Preboreal oscillation) can be inferred from the stable isotope record from Plinz [88] and from Bleßberg Cave [89]. Lake Jues records indicate a cooling phase culminating between ca. 10,550 and 10,230 cal BP (bond event 7, Boreal cooling), with frequent flooding during the spring [90]. Again, the Bleßberg Cave record [89] suggests cooling and drying and/or increased winter precipitation prior to the prominent 8.2 ka event [101], followed by the return of permafrost conditions from 8.26 to 7.85 ka BP. Lake Jues records additionally indicate higher springtime precipitation occurring between 8.2 and 7.5 cal ka BP [90].

Further relevant geomorphic information for the Preboreal to early Atlantic period can be inferred from the laboratory results derived from the sampled drilling core UA19_5a (Figure 7). Here, the uppermost sections of the basal overbank fines (5.08 to 5.18 m) show increased TOC (2.8%) and reduced $CaCO_3$ values (0.6%) compared with the basal overbank fines below. This might be a result of organic matter accumulation and substrate decalcification, two well-known processes of initial soil formation [102,103]. Supporting evidence for initial soil comes from the grain size results. Here, increased clay contents (19.0%) may reflect in situ mineral weathering and clay mineral formation. Furthermore, the calculated ΔGSD value is noticeably higher in these sections (1.1%), also indicating post-depositional chemical weathering (pedogenesis) and enrichment of the secondarily formed clay minerals related to pedogenic processes [69]. Similar but less clear results from basal overbank fines at UA19_8a (Figure 8, 4.33 to 5.08 m) indicate a degree of floodplain stability associated with reduced flooding and initial soil formation after the deposition of basal overbank fines during the early Holocene.

5.1.3. Early Atlantic to Late Subboreal Rieth Formation with Intercalated Overbank Fines

Peat and tufa ("rieth series") deposits indicate a poorly drained Unstrut floodplain at this evolutionary stage (Figure 4). Considering the paludal model [104], several ephemeral ponds may have existed, promoting the establishment of mixed flora and fauna within the Unstrut floodplain. Our dating results provide evidence that such floodplain conditions were already locally (UA19_6) established in the Preboreal period (11,004 ± 192 cal BP). However, these conditions became dominant in the entire Unstrut floodplain during the early Atlantic to late Subboreal period (approx. 7.3 to 3.4 cal ka BP), in line with nearby findings [47]. Based on our data, the formation of thick basal peat layers, preserved in the lower section of the "rieth series" deposits, ended around 6.4 cal ka BP, as indicated by two well-matching ^{14}C ages (6404 ± 88 and 6347 ± 49 cal BP) from the upper peat boundary of cores Gro16 and UA19_7 (Figures 4 and 5). Afterwards tufa formation became dominant, interfingered by rather thin peat layers. Four ^{14}C datings from peat layers preserved in the upper rieth section yielded coinciding ages of 3360 ± 89 cal BP (UA19_7), 3412 ± 42 cal BP (UA19_4), 3536 ± 83 cal BP (See16), and 3873 ± 97 cal BP (UA19_8a), terminating the end of "rieth series" formation in the upper Unstrut catchment not considerably later than 3.4 cal ka BP. Geomorphologically, the peat and tufa deposits clearly indicate wetland or telmatic conditions and can be considered a terrestrial response to overall mid-Holocene climatic amelioration in Central Europe [89–91,105,106]. However, the appearance of the decomposed and highly decomposed peat is attributed to hydrologically unfavourable

conditions, possibly with periodic sediment input by flooding [107,108]. The tufa deposits generally indicate discharge dominated by dissolved load, leading to tufa precipitation around the established floodplain vegetation [104]. In contrast, suspended sediment transfer into the Unstrut floodplain was limited in periods of peat and tufa formation. This generally indicates reduced sediment supply from the catchment, maybe due to erosion control by a well-established vegetation cover [84].

However, temporally in line with nearby floodplain studies reporting fine-clastic sediment deposited during the Atlantic period [109,110], our results indicate that "rieth series" formation was interrupted by phases of increased sediment input. This is shown by the deposition of intercalated overbank fines, which were ^{14}C-dated to 4853 ± 22 cal BP (UA19_5a) and 4845 ± 18 cal BP (UA19_7). Considering the aforementioned ^{14}C ages from the covering peat layers (3360 ± 89 cal BP, 3412 ± 42 cal BP, and 3873 ± 97 cal BP), this phase of overbank sedimentation may have continued until the late Subboreal period (around 3.4 cal ka BP). Further supporting evidence for increased sediment input into the Unstrut floodplain during the early Subboreal period comes from drilling site UA19_8a (Figure 8). Here, three almost equal ^{14}C ages (5130 ± 153, 5256 ± 185 and 5135 ± 155) taken between 3.6 and 4.3 m indicate the very fast filling of a surveyed paleochannel after 5.1 cal ka BP.

A lack of evidence for pronounced climate changes in the region during the corresponding early to late Subboreal period (5.1 to 3.4 cal ka BP) indicates a mainly non-climate-related explanation for increased overbank sedimentation and the fast paleochannel infilling. In this context, it seems most plausible that sediment input originates from anthropogenic soil erosion in the catchment, since the upper Unstrut catchment was intensively settled and used from the early Neolithic period [49,50]. The deposition period lies in the late to end-Neolithic and early Bronze Age cultural periods, for which numerous settlement sites directly bordering the course of the Unstrut River are evident (Figure 2A,B) and striking advances in technological and economic development are well-known [50,110]. Considerable anthropogenic soil erosion and increased sediment delivery to the Unstrut channel are therefore very likely for these periods. Eroded soils were at least partly deposited as overbank fines or paleochannel infillings in the Unstrut floodplain. In this context, the fairly short distance from the settlement and farming sites to the Unstrut channel resulted in comparatively high hydro-sedimentary connectivity [16], promoting a relatively fast sediment transfer into the floodplain. Compared with other Central European floodplains, this is relatively early for the start of human-triggered overbank sedimentation [10,12,17,111]. A spatial concentration of known early to middle Neolithic sites at a larger distance to the Unstrut floodplain (Figure 2A) would therefore be a possible explanation for the lack of overbank fines from these earlier land-use periods.

As discussed for the basal overbank fines (Section 5.1.2), laboratory analysis of the overbank fines intercalated in the "rieth series" also provides hints concerning initial soil formation prior to subsequent sediment coverage. This is the case for overbank deposits from core UA19_5a (3.8 to 4.1 m). Here, increased TOC content (7.2%) goes along with a comparatively reduced $CaCO_3$ value (11.0%), and increased clay content (28.4%) and ΔGSD values (1.7%). Similarly, the section from 2.2 to 2.37 m at drilling site UA19_8a shows increased TOC content (3.3 to 4.5%), relatively low $CaCO_3$ content (3.4 to 4.5%), increased clay content (18.5 to 18.8%), and a comparatively high ΔGSD (1.0%). Once again, these results indicate geomorphic stability in the Unstrut floodplain after overbank sedimentation, in line with limited flooding and initial soil formation.

5.1.4. Late Subboreal to Early Subatlantic Overbank Deposition

Organic overbank fines covering "rieth series" deposits document a further strong sediment input into the Unstrut floodplain. Two chronologically consistent ^{14}C ages from cores UA19_5a (2909 ± 56 cal BP) and UA19_8a (2250 ± 92 cal BP) date this phase of flood loam aggradation in the late Subboreal to early Subatlantic period. This result is roughly in line with the conspicuous period of fluvial activity of other German rivers,

which occurred between approx. 3.4 and 2.8 cal ka BP [10]. Climate conditions during this period might be best described as progressively wet accompanied by considerable temperature fluctuations [112,113]. Furthermore, increased human activities need to be assumed for this period, since numerous settlements and burial finds proximal to the Unstrut floodplain testify an intense occupation and land use by late Bronze and Iron Age cultural groups (Figure 2B,C). In line with large datasets on soil erosion history in Central Europe [100,114], the results indicate that these conditions caused relatively higher soil erosion rates again, followed by increased sediment input into the Unstrut channel and the deposition of mobilized overbank fines by vertical accretion.

After deposition, initial soil formation can be assumed again based on the laboratory data of the sampled drilling cores UA19_5a (2.7 to 3.1 m) and UA19_8a (1.2 to 1.45 m). In both cases the TOC content (2.0 to 5.2%) and clay content (22.7 to 25.5%) was increased and can be referred to as organic matter accumulation and in situ clay mineral formation (Figures 7 and 8). This interpretation is supported by the increased ΔGSD (~0.8%) from core UA19_5a, also indicating post-depositional chemical weathering and an enrichment of secondarily formed clay minerals related to pedogenic processes [69].

5.1.5. Latest Holocene Overbank Deposition and Colluviation

Up to 2.7 m thick overbank fines indicate a further period of substantial soil erosion and sediment transfer into the Unstrut floodplain. Three charcoal ^{14}C datings provide ages of 1009 ± 49 cal BP (UA19_8a), 880 ± 80 cal BP (UA19_5), and 601 ± 49 cal BP (UA19_8a), locating overbank deposition in the High and late Medieval period (11th to 14th century CE). This is chronologically supported by four OSL datings from the investigated site SG19_1a (Table 2). The OSL ages of 0.76 ± 0.16, 0.73 ± 0.15, 0.61 ± 0.05, and 0.69 ± 0.07 ka point to floodplain deposition in just around 150 years during the late Medieval period (13th to 15th century CE).

For the upper Unstrut catchment, territorial expansion and settlement foundation started in the late 8th and 9th centuries CE, but began on a large scale around the year 1100 CE [51]. This process was linked to deforestation, so that for instance some of the building timber for the churches of the nearby city of Mühlhausen (Figure 1B) had to be rafted from the Thuringian Forest [115]. Additionally, agrarian intensification must be assumed, leading to accelerated soil erosion, intense suspended sediment influx into the Unstrut River, and thus strongly increased floodplain deposition. Early and high Medieval climate conditions (before around 1200 cal BP) were warm and humid, with only few fluctuations [113,116]. During the 13th and 14th centuries CE, wetter summers and a first cold spell (approx. 1300 cal CE) document the onset of the Little Ice Age [113]. This overall climatic change was accompanied by several extreme precipitation events during the 14th century (e.g., 1342/43 CE), which should also have impacted the region [52,117–119]. As especially indicated by the OSL ages, erosion rates may have been extraordinarily high during these extreme precipitation events. In contrast to this, this study does not so far provide evidence for substantial overbank deposition during modern times, even though severe flooding events (e.g., 1613, 1815, 1852) are historically well-documented for the Unstrut catchment [40,41] and related sedimentation must be expected. Corresponding overbank fines from these flooding events might form the uppermost approx. 0.5 m and have been mixed up by constant ploughing.

In summary, this study indicates that strong overbank aggradation in the upper Unstrut floodplain occurred when the climax of settlement foundation, large-scale deforestation, and substantial land-use intensification went in hand with generally wet climate conditions and frequently heavy precipitation events. The reconstruction of increased sedimentation during the Medieval period is generally in agreement with the regional [42,44,47,108] and supra-regional [10,11,17] pattern of floodplain deposition.

Slight post-sedimentary alteration of the uppermost overbank fines can be inferred from selected laboratory results of the sampled cores (UA19_5a, UA19_8a, SG19_1a). Core UA19_5a shows a decreasing $CaCO_3$ content in the uppermost 1.8 m, which might be

related to decalcification (Figure 7). Additionally, this zone shows higher ΔGSD values (up to 0.8%), indicating enrichment of secondarily formed clay minerals. Similarly, ΔGSD is increased (0.6 to 1.5%) in the uppermost overbank fines of the drilling core SG19_1a with a maximum around 1.1 m below the surface (Figure 6). This goes along with a higher TOC content (1.1 to 1.4%) in this section that may be caused by organic matter accumulation.

6. Conclusions

This case study considered the late Pleistocene and Holocene fluvial evolution of the upper Unstrut floodplain, a loess region in the climatic transitional zone from an oceanic to a more continental climate. The chronostratigraphy is relatively continuous, resulting in the Unstrut deposits having a high archive potential. In this context, the extensive aggradation and preservation of fluvial sediments is possibly related to pronounced hillslope to floodplain connectivity and the relatively wide valley situation in the upper Unstrut section.

The results suggest that floodplain development in the late Pleistocene and early Holocene (Preboreal to early Atlantic period) was considerably controlled by climatic conditions and short-term climate variabilities which caused gravel deposition (around 11.6 cal ka BP) and overbank sedimentation (between 11.6 and 7.0 cal ka BP).

Afterwards, floodplain conditions varied between active and stable periods. The reconstructed phases of increased sediment input into the floodplain (active period) temporally correspond well with increased land-use phases during the late Neolithic to early Bronze Age period (5.1 to 3.4 cal ka BP), late Bronze to Iron Age period (2.9 to 2.3 cal ka BP), and high to late Medieval period (1.0 to 0.6 cal ka BP). Obviously, floodplain evolution was strongly influenced by settlement dynamics in addition to climatic conditions and short-term climate changes. In contrast, stable periods are characterized by peat and tufa formation ("rieth series") as well as initial soil formation, which is particularly detectable in the overbank deposits. In this context, initial soil formation includes organic matter accumulation (increase in TOC), substrate decalcification (decrease in $CaCO_3$), and clay mineral formation (increase in clay content and ΔGSD).

Summing up, this floodplain study from the Central European climate boundary is in general agreement with the known fluvial patterns of western and Central European river systems. However, it indicates that this transitional zone has been very geomorphologically vulnerable to natural and human-induced changes during the latest Pleistocene and Holocene. This high level of vulnerability to external impacts, which are expected to become even more important with future climate change, should be considered in future river predictions and river and floodplain management.

Supplementary Materials: The following supporting information can be downloaded at: https://www.mdpi.com/article/10.3390/geosciences12080310/s1, Table S1: Laboratory results core SG19_1a, UA19_5a, and UA19_8a.

Author Contributions: Conceptualization, A.K. and J.K.; methodology, J.K., P.S., T.W. and T.L.; investigation, A.K., J.K., P.S. and T.L.; data curation, A.K. and J.K.; writing—original draft preparation, A.K. and J.K.; visualization, J.K., P.S., T.W. and A.K.; supervision, A.K.; project administration, A.K. All authors have read and agreed to the published version of the manuscript.

Funding: This research received no external funding.

Institutional Review Board Statement: Not applicable.

Informed Consent Statement: Not applicable.

Data Availability Statement: The datasets generated during and/or analysed during the current study are available from the corresponding author on reasonable request.

Acknowledgments: We sincerely thank the two reviewers for the thorough revision of our manuscript and their constructive comments that helped to improve the paper. Furthermore, we acknowledge the editor for handling this paper. Moreover, the authors are very grateful to the help of the students' initiative BokuHiLa (Bodenkunde Hildesheimer Land) for supporting the fieldwork. In addition, we

thank Anne-Kathrin Nüsch for guiding ERT field investigations as well as Michael Gräber (GeoServe Angewandte Geophysik) for providing the RESECS equipment. Wulf Walther and Mario Küßner are acknowledged for sharing their extensive archaeological expertise. Last but not least, Katharine Thomas is acknowledged for improving the language of the manuscript.

Conflicts of Interest: The authors declare no conflict of interest.

References

1. Fischer, P.; Jöris, O.; Fitzsimmons, K.E.; Vinnepand, M.; Prud'homme, C.; Schulte, P.; Hatté, C.; Hambach, U.; Lindauer, S.; Zeeden, C.; et al. Millennial-scale terrestrial ecosystem responses to Upper Pleistocene climatic changes: 4D-reconstruction of the Schwalbenberg Loess-Palaeosol-Sequence (Middle Rhine Valley, Germany). *Catena* **2021**, *196*, 104913. [CrossRef]
2. Theuerkauf, M.; Blume, T.; Brauer, A.; Dräger, N.; Feldens, P.; Kaiser, K.; Kappler, C.; Kästner, F.; Lorenz, S.; Schmidt, J.; et al. Holocene lake-level evolution of Lake Tiefer See, NE Germany, caused by climate and land cover changes. *Boreas* **2022**, *51*, 299–316. [CrossRef]
3. Kaiser, K.; Lorenz, S.; Germer, S.; Joschus, O.; Küster, M.; Libra, J.; Bens, O.; Hüttl, R. Late Quaternary evolution of rivers, lakes and peatlands in northeast Germany reflecting past climatic and human impact—An overview. *EG Quat. Sci. J.* **2012**, *61*, 103–132. [CrossRef]
4. Ghilardi, M.; Cordier, S.; Carozza, J.-M.; Psomiadis, D.; Guilaine, J.; Zomeni, Z.; Demory, F.; Delanghe-Sabatier, D.; Vella, M.-A.; Bony, G.; et al. The Holocene fluvial history of the Tremithos river (south central Cyprus) and its linkage to archaeological records. *Environ. Archaeol.* **2015**, *20*, 184–201. [CrossRef]
5. Kirchner, A.; Nehren, U.; Behling, H.; Heinrich, J. Mid- and Late Holocene fluvial dynamics in the tropical Guapi—Macacu catchment, Southeast Brazil: The role of climate change and human impact. *Palaeogeogr. Palaeoclimatol. Palaeoecol.* **2015**, *426*, 308–318. [CrossRef]
6. von Suchodoletz, H.; Menz, M.; Kühn, P.; Sukhishvili, L.; Faust, D. Fluvial sediments of the Algeti River in southeastern Georgia —An archive of Late Quaternary landscape activity and stability in the Transcaucasian region. *Catena* **2016**, *130*, 95–107. [CrossRef]
7. Faust, D.; Wolf, D. Interpreting drivers of change in fluvial archives of the Western Mediterranean—A critical view. *Earth-Sci. Rev.* **2017**, *174*, 53–83. [CrossRef]
8. Depreux, B.; Lefèvre, D.; Berger, J.-F.; Segaoui, F.; Boudad, L.; El Harradji, A.; Degeai, J.-P.; Limondin-Lozouet, N. Alluvial records of the African Humid Period from the NW African highlands (Moulouya basin, NE Morocco). *Quat. Sci. Rev.* **2021**, *255*, 106807. [CrossRef]
9. Kalis, A.J.; Merkt, J.; Wunderlich, J. Environmental changes during the Holocene climatic optimum in central Europe—Human impact and natural causes. *Quat. Sci. Rev.* **2003**, *22*, 33–79. [CrossRef]
10. Hoffmann, T.; Lang, A.; Dikau, R. Holocene river activity: Analysing ^{14}C-dated fluvial and colluvial sediments from Germany. *Quat. Sci. Rev.* **2008**, *27*, 2031–2040. [CrossRef]
11. Notebaert, B.; Verstraeten, G. Sensitivity of West and Central European river systems to environmental changes during the Holocene: A review. *Earth-Sci. Rev.* **2010**, *103*, 163–182. [CrossRef]
12. Brown, A.G.; Lespez, L.; Sear, D.A.; Macaire, J.-J.; Houben, P.; Klimek, K.; Brazier, R.E.; Van Oost, K.; Pears, B. Natural vs. anthropogenic streams in Europe: History, ecology and implications for restoration, river-rewilding and riverine ecosystem services. *Earth-Sci. Rev.* **2018**, *180*, 185–205. [CrossRef]
13. Stouthamer, E.; Berendsen, H.J.A. Avulsion: The relative roles of autogenic and allogenic processes. Sediment. *Geology* **2007**, *198*, 309–325. [CrossRef]
14. Vandenberghe, J.; Cordier, S.; Bridgland, D. Extrinsic and intrinsic forcing of fluvial development: Understanding natural and anthropogenic influences. *Proc. Geol. Assoc.* **2010**, *121*, 107–112. [CrossRef]
15. Van De Wiel, M.J.; Coulthard, T.J. Self-organized criticality in river basins: Challenging sedimentary records of environmental change. *Geology* **2010**, *38*, 87–90. [CrossRef]
16. Houben, P.; Schmidt, M.; Mauz, B.; Stobbe, A.; Lang, A. Asynchronous Holocene colluvial and alluvial aggradation: A matter of hydrosedimentary connectivity. *Holocene* **2013**, *23*, 544–555. [CrossRef]
17. Notebaert, B.; Broothaerts, N.; Verstraeten, G. Evidence of anthropogenic tipping points in fluvial dynamics in Europe. *Glob. Planet. Chang.* **2018**, *164*, 27–38. [CrossRef]
18. Rommens, T.; Verstraeten, G.; Poesen, J.; Govers, G.; Van Rompaey, A.; Peeters, I. Soil erosion and sediment deposition in the Belgian loess belt during the Holocene: Establishing a sediment budget for a small agricultural catchment. *Holocene* **2005**, *15*, 1032–1043. [CrossRef]
19. Broothaerts, N.; Notebaert, B.; Verstraeten, G.; Kasse, C.; Bohncke, S.; Vandenberghe, J. Non-uniform and diachronous Holocene floodplain evolution: A case study from the Dijle catchment, Belgium. *J. Quat. Sci.* **2014**, *29*, 351–360. [CrossRef]
20. Notebaert, B.; Verstraeten, G.; Rommens, T.; Vanmontfort, B.; Govers, G.; Poesen, J. Establishing a Holocene sediment budget for the river Dijle. *Catena* **2009**, *77*, 150–163. [CrossRef]
21. Pastre, J.-F.; Limondin-Lozouet, N.; Gebhardt, A.; Leroyer, C.; Fontugne, M.; Krier, V. Lateglacial and Holocene fluvial records from the central part of the Paris Basin (France). In *River Basin Sediment Systems—Archives of Environmental Change*; Maddy, D., Macklin, M.G., Woodward, J.C., Eds.; Balkema: Rotterdam, The Netherlands, 2001; pp. 357–373; ISBN 9789058093424.

22. Lespez, L.; Clet-Pellerin, M.; Limondin-Lozouet, N.; Pastre, J.-F.; Fontugne, M.; Marcigny, C. Fluvial system evolution and environmental changes during the Holocene in the Mue valley (Western France). *Geomorphology* **2008**, *98*, 55–70. [CrossRef]
23. Andres, W.; Bos, J.A.A.; Houben, P.; Kalis, A.J.; Nolte, S.; Rittweger, H.; Wunderlich, J. Environmental change and fluvial activity during the Younger Dryas in Central Germany. *Quat. Int.* **2001**, *79*, 89–100. [CrossRef]
24. Houben, P. Sediment budget for five millennia of tillage in the Rockenberg catchment (Wetterau loess basin, Germany). *Quat. Sci. Rev.* **2012**, *52*, 12–23. [CrossRef]
25. Houben, P. Scale linkage and contingency effects of field-scale and hillslope-scale controls of long-term soil erosion: Anthropogeomorphic sediment flux in agricultural loess watersheds of southern Germany. *Geomorphology* **2008**, *101*, 172–191. [CrossRef]
26. Schmidt-Wygasch, C.; Schamuhn, S.; Meurers-Balke, J.; Lehmkuhl, F.; Gerlach, R. Indirect Dating of Historical Land Use Through Mining: Linking Heavy Metal Analyses of Fluvial Deposits to Archaeobotanical Data and Written Accounts. *Geoarchaeology* **2010**, *25*, 837–857. [CrossRef]
27. Tinapp, C.; Meller, H.; Baumhauer, R. Holocene accumulation of colluvial and alluvial sediments in the Weiße Elster River valley in Saxony, Germany. *Archaeometry* **2008**, *50*, 696–709. [CrossRef]
28. Tinapp, C.; Heinrich, S.; Herbig, C.; Schneider, B.; Stäuble, H.; Miera, J.; von Suchodoletz, H. Holocene floodplain evolution in a central European loess landscape—geoarchaeological investigations of the lower Pleiße valley in NW-Saxony. *EG Quat. Sci. J.* **2019**, *68*, 95–105. [CrossRef]
29. Ballasus, H.; Schneider, B.; von Suchodoletz, H.; Miera, J.; Werban, U.; Fütterer, P.; Werther, L.; Ettel, P.; Veit, U.; Zielhofer, C. Overbank silt-clay deposition and intensive Neolithic land use in a Central European catchment—Coupled or decoupled? *Sci. Total Environ.* **2022**, *806*, 150858. [CrossRef]
30. von Suchodoletz, H.; Pohle, M.; Khosravichenar, A.; Ulrich, M.; Hein, M.; Tinapp, C.; Schultz, J.; Ballasus, H.; Veit, U.; Ettel, P.; et al. The fluvial architecture of buried floodplain sediments of the Weiße Elster River (Germany) revealed by a novel method combination of core drillings with 2D and 3D geophysical measurements. *Earth Surf. Process. Landf.* **2022**, *47*, 955–976. [CrossRef]
31. Starkel, L. Role of climatic and anthropogenic factors accelerating soil erosion and fluvial activity. *Stud. Quat.* **2005**, *22*, 27–33.
32. Starkel, L.; Kalicki, T.; Krapiec, M.; Soja, R.; Gebica, P.; Czyzowska, E. Hydrological changes of valley floors in upper Vistula basin during late Vistulian and Holocene. In *Evolution of the Vistula River Valley During the Last 15000 Years*; Starkel, L., Ed.; Geographical Studies: Wrocław, Poland, 1996; pp. 7–128.
33. Langbein, R. *Keuper. Geologie von Thüringen*, 3rd ed.; Seidel, G., Ed.; Schweizerbart: Stuttgart, Germany, 2003; pp. 357–391; ISBN 9783510652051.
34. Lehmkuhl, F.; Nett, J.J.; Pötter, S.; Schulte, P.; Sprafke, T.; Jary, Z.; Antoine, P.; Wacha, L.; Wolf, D.; Zerboni, A.; et al. Loess landscapes of Europe—Mapping, geomorphology, and zonal differentiation. *Earth-Sci. Rev.* **2021**, *215*, 103496. [CrossRef]
35. Zöller, L.; Rousseau, D.-D.; Jäger, K.-D.; Kukla, G. Last interglacial, Lower and Middle Weichselian—A comparative study from the Upper Rhine and Thuringian loess areas. *Z. Geomorphol.* **2004**, *48*, 1–24. [CrossRef]
36. Schramm, H.A. Böden. In *Geologie von Thüringen*, 3rd ed.; Seidel, G., Ed.; Schweizerbart: Stuttgart, Germany, 2003; pp. 530–548; ISBN 9783510652051.
37. Karaschewski, J.; Kirchner, A. Erste Ergebnisse zur Bodenentwicklung und Kolluviationsgeschichte am "Kobenkopf" (Unstrut-Hainich-Kreis). *Mühlhäuser Beiträge* **2018**, *41*, 73–90.
38. Peel, M.C.; Finlayson, B.L.; McMahon, T.A. Updated world map of the Köppen-Geiger climate classification. *Hydrol. Earth Syst. Sci.* **2007**, *11*, 1633–1644. [CrossRef]
39. Hiekel, W.; Tinz, B. Klima. In *Der Hainich. Eine landeskundliche Bestandsaufnahme im Raum Mühlhausen, Bad Langensalza, Schlotheim, Großengottern, Mihla und Behringen*; Großmann, M., John, U., Porada, H.T., Eds.; Landschaften in Deutschland 77; Böhlau Verlag: Köln/Weimar, Germany, 2018; pp. 23–27; ISBN 9783412223007.
40. Militzer, S.; Glaser, R. Die Thüringische Sintflut von 1613. Z. Ver. *Thüringische Gesch.* **1994**, *48*, 69–92.
41. Deutsch, M.; Pörtge, K.H. *Hochwasser in Thüringen. Ursachen, Verlauf und Schäden Extremer Abflussereignisse (1500–2015)*; Schriftenreihe der Thüringer Landesanstalt für Umwelt und Geologie (TLUG): Jena, Germany, 2017; p. 113.
42. Jäger, K.-D. Über Alter und Ursachen der Auelehmablagerung thüringischer Flüsse. *Prähistorische Zeitschrift* **1962**, *40*, 1–59. [CrossRef]
43. Lange, E.; Schultz, A. Pollenanalytische Datierung spätglazialer und holozäner Sedimente im Zentralen Thüringer Becken. *Wiss. Zeitschr. Univ. Jena Math—Nat. Reihe* **1965**, *14*, 45–53.
44. Unger, K.P.; Rau, D. Zur Gliederung und Entwicklung der rezenten Talauen des zentralen Thüringer Beckens—Ergebnisse der geologisch-bodenkundlichen Aufnahme des Meßtischblattes Weißensee. *Jahrbuch Geol.* **1965**, *1*, 395–410.
45. Kliewe, H.; Schultz, A. Zur Talgenese seit dem Spätglazial im inneren Thüringer Becken. *Acta Geogr. Debrecina* **1968**, *T XIV*, 115–123.
46. Suderlau, G. Jungquartäre Ablagerungen in den Senken des Raumes Eisleben—Artern—Bad Frankenhausen. *Hercynia N.F.* **1975**, *12*, 228–255.
47. Bischoff, R. Untersuchungen an spätglazialen und holozänen Auensedimenten des Unstruttals im Bereich des zentralen Thüringer Beckens. *Geowissenschaftliche Mitteilungen Thüringen* **1999**, *7*, 127–141.
48. Unger, K.P. Quartär. In *Geologie von Thüringen*, 3rd ed.; Seidel, G., Ed.; Schweizerbart: Stuttgart, Germany, 2003; pp. 424–443; ISBN 9783510652051.

49. Küßner, M. Erster Bericht zu den Gräbern der Linienbandkeramik mit Spondylus-Artefakten von Höngeda (Unstrut-Hainich-Kreis). *Mühlhäuser Beiträge* **2017**, *40*, 49–62.
50. Walther, W. Archäologie. In *Der Hainich. Eine landeskundliche Bestandsaufnahme im Raum Mühlhausen, Bad Langensalza, Schlotheim, Großengottern, Mihla und Behringen*; Großmann, M., John, U., Porada, H.T., Eds.; Landschaften in Deutschland 77; Böhlau Verlag: Köln/Weimar, Germany, 2018; pp. 60–71; ISBN 9783412223007.
51. Schirmer, U. Historische Entwicklung im Mittelalter. In *Der Hainich. Eine landeskundliche Bestandsaufnahme im Raum Mühlhausen, Bad Langensalza, Schlotheim, Großengottern, Mihla und Behringen*; Großmann, M., John, U., Porada, H.T., Eds.; Landschaften in Deutschland 77; Böhlau Verlag: Köln/Weimar, Germany, 2018; pp. 71–84; ISBN 9783412223007.
52. Bork, H.R.; Bork, H.; Dalchow, C.; Faust, B.; Piorr, H.P.; Schatz, T. *Landschaftsentwicklung in Mitteleuropa—Wirkung des Menschen auf Landschaften*; Klett-Perthes: Gotha, Germany, 1998; p. 328; ISBN 9783623008493.
53. Schirmer, U. Neuzeitliche Entwicklung bis 1800. In *Der Hainich. Eine landeskundliche Bestandsaufnahme im Raum Mühlhausen, Bad Langensalza, Schlotheim, Großengottern, Mihla und Behringen*; Großmann, M., John, U., Porada, H.T., Eds.; Landschaften in Deutschland 77; Böhlau Verlag: Köln/Weimar, Germany, 2018; pp. 84–89; ISBN 9783412223007.
54. Schöne, J. *Die Landwirtschaft der DDR 1945–1990*; Landeszentrale für Politische Bildung Thüringen: Erfurt, Germany, 2015; p. 80; ISBN 393142690-4.
55. Behm-Blancke, G.; Jacob, H.; Ullrich, H.; Eberhardt, H. *Heiligtümer der Germanen und Ihrer Vorgänger in Thüringen: Die Kultstätte Oberdorla: Forschungen zum Alteuropäischen Religions-und Kultwesen. Weimarer Monographien zur Ur- und Frühgeschichte 38*; Konrad Theiss: Stuttgart, Germany, 2003; p. 280; ISBN 3806218110.
56. Knödel, K.; Krummel, H.; Lange, G. *Handbuch zur Erkundung des Untergrundes von Deponien und Altlasten—Band 3: Geophysik*, 2nd ed.; Bundesanstalt für Geowissenschaften und Rohstoffe; Springer: Berlin/Heidelberg, Germany, 2005; p. 1063; ISBN 9783662077245.
57. Rücker, C.; Günther, T.; Wagner, F.M. pyGIMLi: An open-source library for modelling and inversion in geophysics. *Comput. Geosci.* **2017**, *109*, 106–123. [CrossRef]
58. Karaschewski, J. Auensedimente als Geoarchiv der Landschaftsgeschichte–Ein Fallbeispiel aus dem Oberen Unstruteinzugsgebiet (NW-Thüringen). Master's Thesis, University of Hildesheim, Hildesheim, Germany, 2016; p. 87, *unpuplished Masterthesis*.
59. Ad-hoc-Arbeitsgruppe Boden. *Bodenkundliche Kartieranleitung*, 5th ed.; Schweizerbart Science Publishers: Stuttgart, Germany, 2005; ISBN 9783510959204.
60. Munsell Color Company. *Munsell Soil Color Charts*; Revised Edition; Macbeth Division of Kollmorgen: New Windsor, NY, USA, 1994.
61. Eckmeier, E.; Egli, M.; Schmidt, M.W.I.; Schlumpf, N.; Nötzli, M.; Minikus-Stary, N.; Hagedorn, F. Preservation of fire-derived carbon compounds and sorptive stabilisation promote the accumulation of organic matter in black soils of the Southern Alps. *Geoderma* **2010**, *159*, 147–155. [CrossRef]
62. Zeeden, C.; Krauß, L.; Kels, H.; Lehmkuhl, F. Digital image analysis of outcropping sediments: Comparison to photospectrometric data from Quaternary loess deposits at Şanoviţa (Romania) and Achenheim (France). *Quat. Int.* **2017**, *429*, 100–107. [CrossRef]
63. Sprafke, T. *Löss in Niederösterreich. Archiv quartärer Klima- und Landschaftsveränderungen*; Würzburg University Press: Würzburg, Germany, 2016; p. 272. [CrossRef]
64. Thielicke, G. Zusammenstellung einiger wichtiger bodenchemischer und –mechanischer Laboratoriumsmethoden, ihre Anwendungen, Ergebnisdarstellungen und Fehlerquellen. *Geologisches Jahrbuch Hessen* **1987**, *115*, 423–448.
65. Blume, H.-P.; Stahr, K.; Leinweber, P. *Bodenkundliches Praktikum*, 3rd ed.; Springer: Berlin/Heidelberg, Germany, 2011; p. 255. [CrossRef]
66. *DIN ISO 11277*; Soil Quality—Determination of Particle Size Distribution in Mineral Soil Material—Method by Sieving and Sedimentation. Beuth-Verlag: Berlin, Germany, 2002.
67. Schulte, P.; Lehmkuhl, F.; Steininger, F.; Loibl, D.; Lockot, G.; Protze, J.; Fischer, P.; Stauch, G. Influence of HCl pretreatment and organo-mineral complexes on laser diffraction measurement of loess-paleosol-sequences. *Catena* **2016**, *137*, 392–405. [CrossRef]
68. Özer, M.; Orhan, M.; Işik, N.S. Effect of Particle Optical Properties on Size Distribution of Soils Obtained by Laser Diffraction. *Environ. Eng. Geosci.* **2010**, *16*, 163–173. [CrossRef]
69. Schulte, P.; Lehmkuhl, F. The difference of two laser diffraction patterns as an indicator for post-depositional grain size reduction in loess-paleosol sequences. *Palaeogeogr. Palaeoclimatol. Palaeoecol.* **2018**, *509*, 126–136. [CrossRef]
70. Hajdas, I. Radiocarbon dating and its applications in Quaternary studies. *EG Quat. Sci. J.* **2008**, *57*, 2–24. [CrossRef]
71. de Vries, H.; Barendsen, G.W. Measurements of age by the carbon-14 technique. *Nature* **1954**, *174*, 1138–1141. [CrossRef]
72. Reimer, P.J.; Austin, W.E.N.; Bard, E.; Bayliss, A.; Blackwell, P.G.; Bronk Ramsey, C.; Butzin, M.; Cheng, H.; Edwards, R.L.; Friedrich, M.; et al. The IntCal20 Northern Hemisphere Radiocarbon Age Calibration Curve (0–55 cal kBP). *Radiocarbon* **2020**, *62*, 725–757. [CrossRef]
73. Murray, A.S.; Wintle, A.G. The single aliquot regenerative dose protocol: Potential for improvements in reliability. *Radiat. Meas.* **2003**, *37*, 377–381. [CrossRef]
74. Antoine, P.; Coutard, S.; Guerin, G.; Deschodt, L.; Goval, E.; Locht, J.-L.; Paris, C. Upper Pleistocene loess-palaeosol records from Northern France in the European context: Environmental background and dating of the Middle Palaeolithic. *Quat. Int.* **2016**, *411*, 4–24. [CrossRef]

75. Sprafke, T.; Schulte, P.; Meyer-Heintze, S.; Händel, M.; Einwögerer, T.; Simon, U.; Peticzka, R.; Schäfer, C.; Lehmkuhl, F.; Terhorst, B. Paleoenvironments from robust loess stratigraphy using high-resolution color and grain-size data of the last glacial Krems-Wachtberg record (NE Austria). *Quat. Sci. Rev.* **2020**, *248*, 106602. [CrossRef]
76. Semmel, A.; Terhorst, B. The concept of the Pleistocene periglacial cover beds in central Europe: A review. *Quat. Int.* **2010**, *222*, 120–128. [CrossRef]
77. Kleber, A.; Terhorst, B. *Mid-Latitude Slope Deposits (Cover Beds)*; Developments in Sedimentology 66; Elsevier: Amsterdam, The Netherlands; Heidelberg, Germany, 2013; p. 320; ISBN 9780444531186.
78. Miall, A.D. *The Geology of Fluvial Deposits*; Springer: Berlin, Germany, 1996; p. 582. [CrossRef]
79. Charlton, R. *Fundamentals of Fluvial Geomorphology*; Routledge: London, UK; New York, NY, USA, 2007; p. 264; ISBN 9780415334549.
80. Geyh, M.A.; Schleicher, H. *Absolute Age Determination. Physical and Chemical Dating Methods and Their Application*; Springer: Berlin, Germany, 1990; p. 505. [CrossRef]
81. Warner, R.B. A proposed adjustment for the 'old wood effect'. In Proceedings of the 2nd Symposium of 14C & Archaeology, Groningen, The Netherlands, 7–11 September 1987; Mook, W., Waterbolk, H., Eds.; PACT 29. 1990; pp. 159–172.
82. Rasmussen, S.O.; Andersen, K.K.; Svensson, A.M.; Steffensen, J.P.; Vinther, B.M.; Clausen, H.B.; Siggaard-Andersen, M.-L.; Johnsen, S.J.; Larsen, L.B.; Dahl-Jensen, D.; et al. A new Greenland ice core chronology for the last glacial termination. *J. Geophys. Res.* **2006**, *111*, D6. [CrossRef]
83. Cheng, H.; Zhang, H.; Spötl, C.; Baker, J.; Sinha, A.; Li, H.; Bartolomé, M.; Moreno, A.; Kathayat, G.; Zhao, J.; et al. Timing and structure of the Younger Dryas event and its underlying climate dynamics. *Proc. Natl. Acad. Sci. USA* **2020**, *117*, 23408–23417. [CrossRef]
84. Rohdenburg, H. *Landscape Ecology, Geomorphology*; Catena: Cremlingen-Destedt, Germany, 1989; p. 220; ISBN 392338114X. Available online: https://www.schweizerbart.de/publications/detail/isbn/9783510653942/Rohdenburg_Landscape_Ecology_Geomorph (accessed on 25 March 2022).
85. Blum, M.D.; Törnqvist, T.E. Fluvial responses to climate and sea-level change: A review and look forward. *Sedimentology* **2000**, *47*, 2–48. [CrossRef]
86. Lipps, S. Fluviatile Dynamik im Mittelwesertal während des Spätglazials und Holozäns. *EG Quat. Sci. J.* **1988**, *38*, 78–86. [CrossRef]
87. Mäusbacher, R.; Igl, M.; Schneider, H. Influence of Late Glacial Climate Changes on Sediment Transport in the River Werra (Thuringia, Germany). *Quat. Int.* **2001**, *79*, 101–109. [CrossRef]
88. Boettger, T.; Hiller, A.; Junge, F.W.; Mania, D.; Kremenetski, K. Lateglacial/Early Holocene environmental changes in Thuringia, Germany: Stable isotope record and vegetation history. *Quat. Int.* **2009**, *203*, 105–112. [CrossRef]
89. Breitenbach, S.F.M.; Plessen, B.; Waltgenbach, S.; Tjallingii, R.; Leonhardt, J.; Jochum, K.P.; Scholz, D. Holocene interaction of maritime and continental climate in Central Europe: New speleothem evidence from central Germany. *Glob. Planet. Chang.* **2019**, *176*, 144–161. [CrossRef]
90. Voigt, R.; Grüger, E.; Baier, J.; Meischner, D. Seasonal variability of Holocene climate: A palaeolimnological study on varved sediments in Lake Jues (Harz Mountains, Germany). *J. Paleolimnol.* **2008**, *40*, 1021–1052. [CrossRef]
91. Schneider, H. Die spät- und Postglaziale Vegetationsgeschichte des Oberen und Mittleren Werratales. In *Paläobotanische Untersuchungen unter Besonderer Berücksichtigung Anthropogener Einflüsse. Dissertationes Botanicae 403*; Gebrüder Borntraeger Verlagsbuchhandlung: Stuttgart, Germany, 2006; p. 229; ISBN 9783443643157.
92. Nanson, G.C.; Croke, J.C. A genetic classification of floodplains. *Geomorphology* **1992**, *4*, 459–486. [CrossRef]
93. Pretzsch, K. *Spätpleistozäne und Holozäne Ablagerungen als Indikator der Fluvialen Morphodynamik im Bereich der Mittleren Leine*; Göttinger Geographische Abhandlungen: Göttingen, Germany, 1994; p. 109; ISBN 9783884520994.
94. Bos, J.A.A.; Urz, R. Lateglacial and early Holocene environment in the middle Lahn river valley (Hessen, central-west Germany) and the local impact of early Mesolithic people—Pollen and macrofossil evidence. *Veget. Hist. Archaeobot.* **2003**, *12*, 19–36. [CrossRef]
95. Urz, R.; Röttger, K.; Thiemeyer, H. Von der Natur- zur Kulturlandschaft. *Germania* **2002**, *80*, 269–293.
96. Dietze, E.; Theuerkauf, M.; Bloom, K.; Brauer, A.; Dörfler, W.; Feeser, I.; Feurdean, A.; Gedminienė, L.; Giesecke, T.; Jahns, S.; et al. Holocene fire activity during low-natural flammability periods reveals scale-dependent cultural human-fire relationships in Europe. *Quat. Sci. Rev.* **2018**, *201*, 44–56. [CrossRef]
97. Bond, G.; Showers, W.; Cheseby, M.; Lotti, R.; Almasi, P.; de Menocal, P.; Priore, P.; Cullen, H.; Hajdas, I.; Bonani, G. A pervasive millenial-scale cycle in North Atlantic Holocene and glacial climates. *Science* **1997**, *278*, 1257–1266. [CrossRef]
98. Mayewski, P.A.; Rohling, E.E.; Stager, J.C.; Karlén, W.; Maasch, K.A.; Meeker, L.D.; Meyerson, E.A.; Gasse, F.; van Kreveld, S.; Holmgren, K.; et al. Holocene climate variability. *Quat. Res.* **2004**, *62*, 243–255. [CrossRef]
99. Giesecke, T.; Bennett, K.D.; Birks, H.J.B.; Bjune, A.E.; Bozilova, E.; Feurdean, A.; Finsinger, W.; Froyd, C.; Pokorný, P.; Rösch, M.; et al. The pace of Holocene vegetation change—Testing for synchronous developments. *Quat. Sci. Rev.* **2011**, *30*, 2805–2814. [CrossRef]
100. Dreibrodt, S.; Lubos, C.; Terhorst, B.; Damm, B.; Bork, H.-R. Historical soil erosion by water in Germany: Scales and archives, chronology, research perspectives. *Quat. Int.* **2010**, *222*, 80–95. [CrossRef]
101. Alley, R.B.; Mayewski, P.A.; Sowers, T.; Stuiver, M.; Taylor, K.C.; Clark, P.U. Holocene climate instability: A prominent widespread event 8200 yr ago. *Geology* **1997**, *25*, 483–486. [CrossRef]

102. Schulte, P.; Hamacher, H.; Lehmkuhl, F.; Esser, V. Initial soil formation in an artificial river valley—Interplay of anthropogenic landscape shaping and fluvial dynamics. *Geomorphology* **2022**, *398*, 108064. [CrossRef]
103. Amelung, W.; Blume, H.-P.; Fleige, H.; Horn, R.; Kandeler, E.; Kögel-Knabner, I.; Kretzschmar, R.; Stahr, K.; Wilke, B.-M. *Scheffer/Schachtschabel Lehrbuch der Bodenkunde*, 17th ed.; Springer: Berlin/Heidelberg, Germany, 2018; p. 750.
104. Pedley, H. Classification and environmental models of cool freshwater tufas. Sediment. *Geology* **1990**, *68*, 143–154.
105. Jäger, K.-D. Oscillations of the water balance during the Holocene in interior Central Europe—Features, dating and consequences. *Quat. Int.* **2002**, *91*, 33–37. [CrossRef]
106. Wanner, H.; Beer, J.; Bütikofer, J.; Crowley, T.J.; Cubasch, U.; Flückiger, J.; Goose, H.; Grosjean, M.; Joos, F.; Kaplan, J.O.; et al. Mid- to Late Holocene climate change: An overview. *Quat. Sci. Rev.* **2008**, *27*, 1791–1828. [CrossRef]
107. Luthardt, V.; Schulz, C.; Meier-Uhlher, R. *Steckbriefe Moorsubstrate*, 2nd ed.; HNE Eberswalde: Berlin, Germany, 2015; p. 154. [CrossRef]
108. Igl, M. Untersuchungen zur spät- und Postglazialen Fluß- und Landschaftsgenese im Mittleren Werratal unter Besonderer Berücksichtigung von Subrosionssenken. Ph.D. Thesis, University of Jena, Jena, Germany, 2000; p. 280.
109. Bebermeier, W.; Holzkämper, P.; Meyer, M.; Schimpf, S.; Schütt, B. Lateglacial to late Holocene landscape history derived from floodplain sediments in context to prehistoric settlement sites of the southern foreland of the Harz Mountains, Germany. *Quat. Int.* **2018**, *463*, 74–90. [CrossRef]
110. Jockenhövel, A. Agrargeschichte der Bronzezeit und vorrömischen Eisenzeit (von ca. 2200 v. Chr. bis Christi Geburt). In *Deutsche Agrargeschichte: Vor und Frühgeschichte*; Henning, F.-W., Ed.; Ulmer: Stuttgart, Germany, 1997; pp. 141–261; ISBN 9783800130993.
111. Stolz, C.; Grunert, J.; Fülling, A. Quantification and dating of floodplain sedimentation in a medium-sized catchment of the German uplands: A case study from the Aar Valley in the southern Rhenish Massif, Germany. *Erde* **2013**, *144*, 30–50. [CrossRef]
112. Bell, M.; Walker, M. *Late Quaternary Environmental Change*, 2nd ed.; Routledge: New York, NY, USA, 2005; p. 348; ISBN 9780130333445.
113. Büntgen, U.; Tegel, W.; Nicolussi, K.; McCormick, M.; Frank, D.C.; Trouet, V.; Kaplan, J.O.; Herzig, F.; Heussner, K.-U.; Wanner, H.; et al. 2500 years of European climate variability and human susceptibility. *Science* **2011**, *331*, 578–582. [CrossRef]
114. Dotterweich, M. The history of soil erosion and fluvial deposits in small catchments of central Europe: Deciphering the long-term interaction between humans and the environment—A review. *Geomorphology* **2008**, *101*, 192–208. [CrossRef]
115. Eißing, T.; Dittmar, C. Timber transport and dendroprovenancing in Thuringia and Bavaria. In *Tree Rings, Art, Archaeology*; Fraiture, P., Ed.; Royal Institute for Cultural Heritage: Brussels, Belgium, 2011; pp. 137–150; ISBN 9782930054131.
116. Negendank, J.F.W. The Holocene: Considerations with regard to its climate and climate archives. In *The Climate in Historical Times. Towards a Synthesis of Holocene Data and Climate Models*; Fischer, H., Kumke, T., Lohmann, G., Flösser, G., Miller, H., Storch, H.V., Negendank, J.F.W., Eds.; Springer: Berlin, Germany, 2004; pp. 1–12; ISBN 9783540206019.
117. Glaser, R. *Klimageschichte Mitteleuropas: 1200 Jahre Wetter, Klima, Katastrophen*; Wissenschaftliche Buchgesellschaft: Darmstadt, Germany, 2013; p. 277; ISBN 978-3896786043.
118. Herget, J.; Kapala, A.; Krell, M.; Rustemeier, E.; Simmer, C.; Wyss, A. The millennium flood of July 1342 revisited. *Catena* **2015**, *130*, 82–94. [CrossRef]
119. Bauch, M. St. Mary Magdelene's Flood (1342) at the intersection of environmental history and the history of infrastructures. *NTM Z. Gesch. Wiss. Tech. Med.* **2019**, *27*, 273–309. [CrossRef]